Chapter 05

Synthesis and biological evaluation of click chemistry-inspired triazole derivatives of natural product molecules for cancer treatment

5 Chapter 05: Synthesis and biological evaluation of click chemistry-inspired triazole derivatives of natural product molecules for cancer treatment

5.1 Introduction and Objective

As per our aim of exploring and enhancing the therapeutic potential of natural product molecules for cancer treatment, we have synthesized and evaluated click chemistry-based triazole derivatives of bioactive natural product molecules for the management of breast cancer in the below-mentioned research work.

5.1.1 Click chemistry and the pharmacological applications of 1,2,3-Triazoles

The click reaction is a standard reaction tool widely exploited for triazole formation. The reaction has successfully been used for the facile synthesis of biologically important molecules. The impact of the click reaction on organic synthesis is reflected in the award of the 2022 Nobel Prize in Chemistry (187).

The emerging field of click chemistry offers a unique approach to the synthesis of 1,2,3-triazole-containing molecules. This reaction owes its usefulness in part to the ease with which azides and alkynes can be introduced into a molecule and their relative stability under a variety of conditions. Azides and alkynes are essentially inert to most biological and organic conditions, molecular oxygen, water, and the majority of common reaction conditions in organic synthesis (141).

1,2,3-triazole moieties are attractive connecting units because they are stable to metabolic degradation and capable of hydrogen bonding, which can be favorable in the binding of biomolecular targets and can improve solubility (188). The 1,2,3-triazole moiety does not occur naturally, although the synthetic molecules containing 1,2,3-triazole units show diverse

biological activities. The importance of triazolic compounds in medicinal chemistry is undeniable.

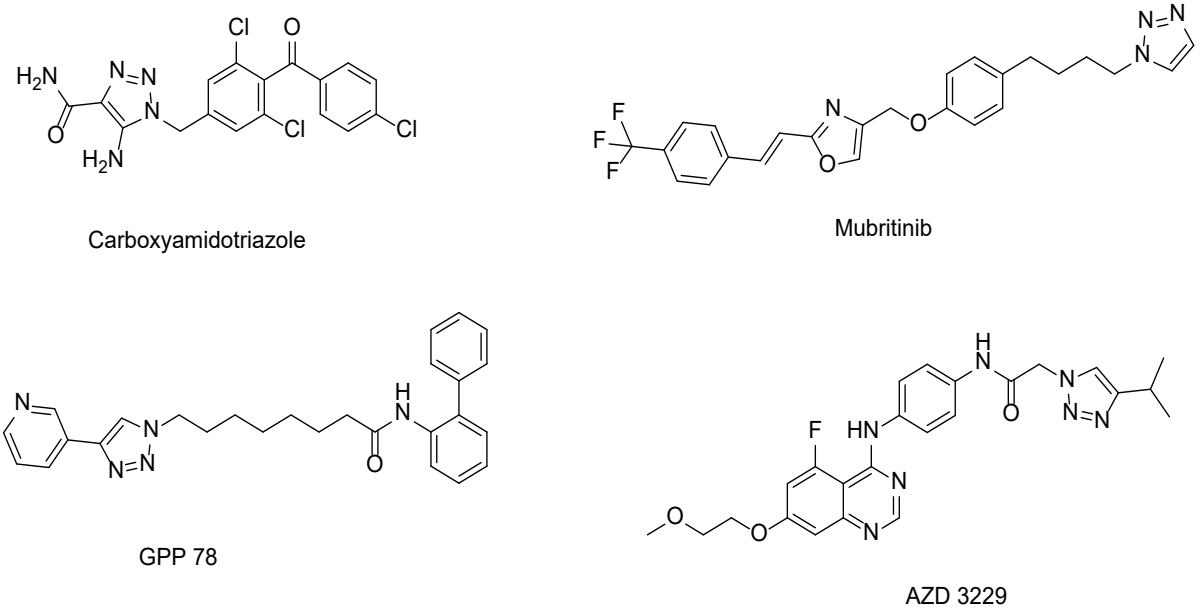

Figure 42 Examples of bioactive anticancer 1,2,3-triazoles

It is well known that 1,2,3-triazole pharmacophores found in a number of biologically active compounds (Fig. 42) possess diverse biological activities such as anti-HIV, antibiotics, antiviral, and anticancer. Based on this core reason, we focused on preparing terpene-based triazole hybrids through a Huisgen 1,3-dipolar cycloaddition reaction (click reaction) of alkynes and azides.

5.2 Experimental work

5.2.1 Materials

All reagents were commercially available. ^{1}H and ^{13}C NMR spectra in $CDCl_3$ and DMSO-d_6 were recorded on Bruker Avance III-500 MHz, using $(CH_3)_4Si$ as an internal standard. Chemical shifts (δ) are expressed in parts per million referenced to the residual solvent (i.e., ^{1}H 7.24 ppm, ^{13}C 77.1 ppm for $CDCl_3$; ^{1}H 2.5 ppm, ^{13}C 49.3 ppm for DMSO-d_6). Signal multiplicity is expressed as follows: s (singlet), br s (broad singlet), d (doublet), t (triplet), q

(quartet), m (multiplet). J values are given in hertz (Hz). For the HRMS measurement, Q-TOF was used. All reactions and purity of the synthesized compounds were monitored by TLC using silica gel 60 F254 aluminium plates. Visualization was accomplished by UV light (254 nm), exposure to iodine vapors, and spraying with p-Anisaldehyde/sulfuric acid followed by heating. Unless otherwise indicated, materials and solvents were purchased and used without further purification.

5.2.2 General synthetic procedures

1,2,3-triazole scaffolds, as ubiquitous structural motifs in different bioactive molecules, pharmaceutical agents, and functional materials, have found wide applications in almost every area of chemistry. In recent decades, several synthetic approaches to these molecules have been explored. Among these, the Cu-catalyzed version of Huisgen's 1,3-dipolar cycloaddition of alkynes and azides has been recognized as an elegant and powerful pathway to access the triazole core.

In their pioneering work, Sharpless et al. reported the Cu(I)-catalyzed, stepwise cycloaddition of azides to terminal alkynes which reveals the broad scope and provides 1,4-disubstituted 1,2,3-triazoles in excellent yields and high regioselectivity (Scheme 01). The chemistry involving copper(I)-catalyzed 1,2,3-triazole formation from azides in the terminal acetylenes is a powerful tool for generating privileged medicinal scaffolds.

This well-known pharmacophore is quite resistant to metabolic degradation and capable of participating in dipole-dipole interactions as well as hydrogen bonding, thus providing additional advantages including cell permeability improvement and target binding (189).

Therefore, we tried to introduce substituted triazoles linkers to Mentha-1,8-diene-7-ol (MDL or PLA) to discover anticancer candidates with better efficacy in this study.

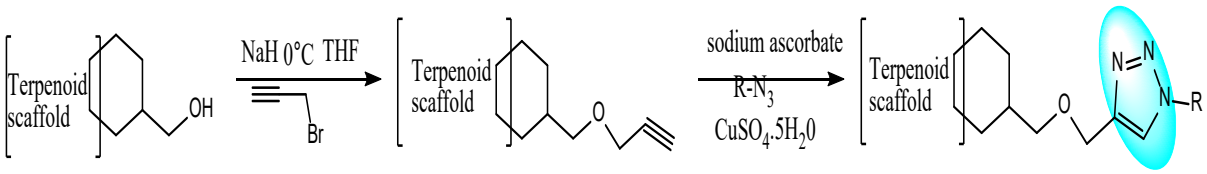

Scheme 01: General scheme for semi-synthetic derivatization of terpenoid moeities

5.2.2.1 General procedure for propargylation of terpenoid moiety

To a solution of NaH (60% dispersion in mineral oil, 1.5 eq.) in THF (30.0 mL) was added to MDL (1.0 eq.) dropwise at 0 ºC. The mixture was warmed up to room temperature and stirred at this temperature for 45 min. At this point, the mixture was cooled to 0 ºC and propargyl bromide solution (80 wt.% in Toluene, 1.5 eq.) was added dropwise. The reaction was warmed up to room temperature for 12 h and quenched by the addition of sat. NH_4Cl (~30 mL) slowly at 0 ºC. The aqueous layer was extracted using Et_2O (3 x 50 mL) and the combined organic layers were washed with brine (3 x 100 mL), dried over Na_2SO_4 and concentrated under reduced pressure on a rotary evaporator to give crude product, which was purified by column chromatography on silica gel using n-hexane: ethyl acetate (90:10 v/v) as eluent to furnish the pure compound 2 as a yellow oil.

5.2.2.2 General procedure for the synthesis of aromatic azides

5.2.2.2.1 Synthesis of aromatic azides from boronic acids

To a suspension of appropriate boronic acids (1.0 eq.) in MeOH (3 mL), in an oven-dried round-bottomed flask, subsequently, $CuSO_4$ (10 mol %) and NaN_3 (1.5 eq.) were added sequentially (Scheme 02). The reaction mixture was stirred vigorously at room temperature for a certain time (monitored by TLC analysis). The resulting mixture was concentrated *in vacuo*, and the residue was extracted with petroleum ether or purified by a pad of silicon gel to give the desired aryl azide (190).

The reaction mixture was quenched with water and extracted with dichloromethane (3 × 50 mL). The organic layer was dried with sodium sulfate and concentrated *in vacuo*. The crude

product was purified using silica gel chromatography with a petroleum ether/dichloromethane gradient to afford the desired products.

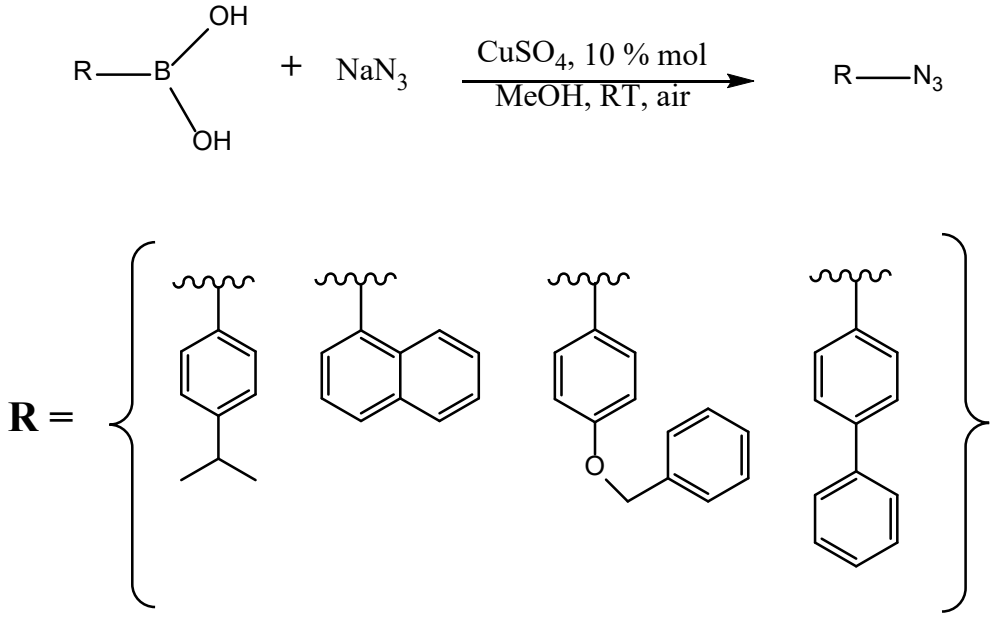

Scheme 02: General scheme for azide synthesis via boronic acids

5.2.2.2.2 Synthesis of aromatic azides from anilines

The aromatic azides are prepared (Scheme 03) by the addition of 6 N HCl solution to stirring dichloromethane solution of the appropriate amine at 0 ºC followed by dropwise addition of saturated aqueous solution of $NaNO_2$ (1.5 eq.), and the contents stirred for 30 min. To the reaction mixture, added NaN_3 (1.5 eq.) and stirred the contents for a further 30 min. The product was then extracted with ethyl acetate (3x 100 mL); the combined organic layers were washed with an aqueous solution of $NaHCO_3$, followed by the brine solution, dried over sodium sulfate, filtered, and concentrated under reduced pressure to give the aryl azides, which were used in the next step without further purification.

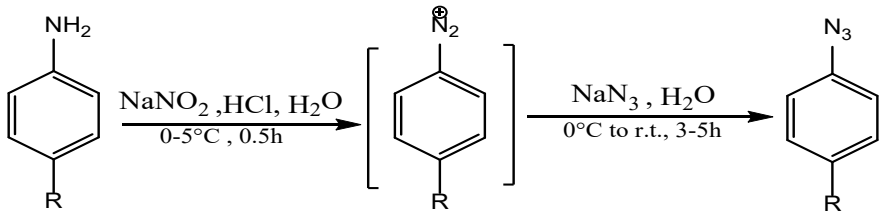

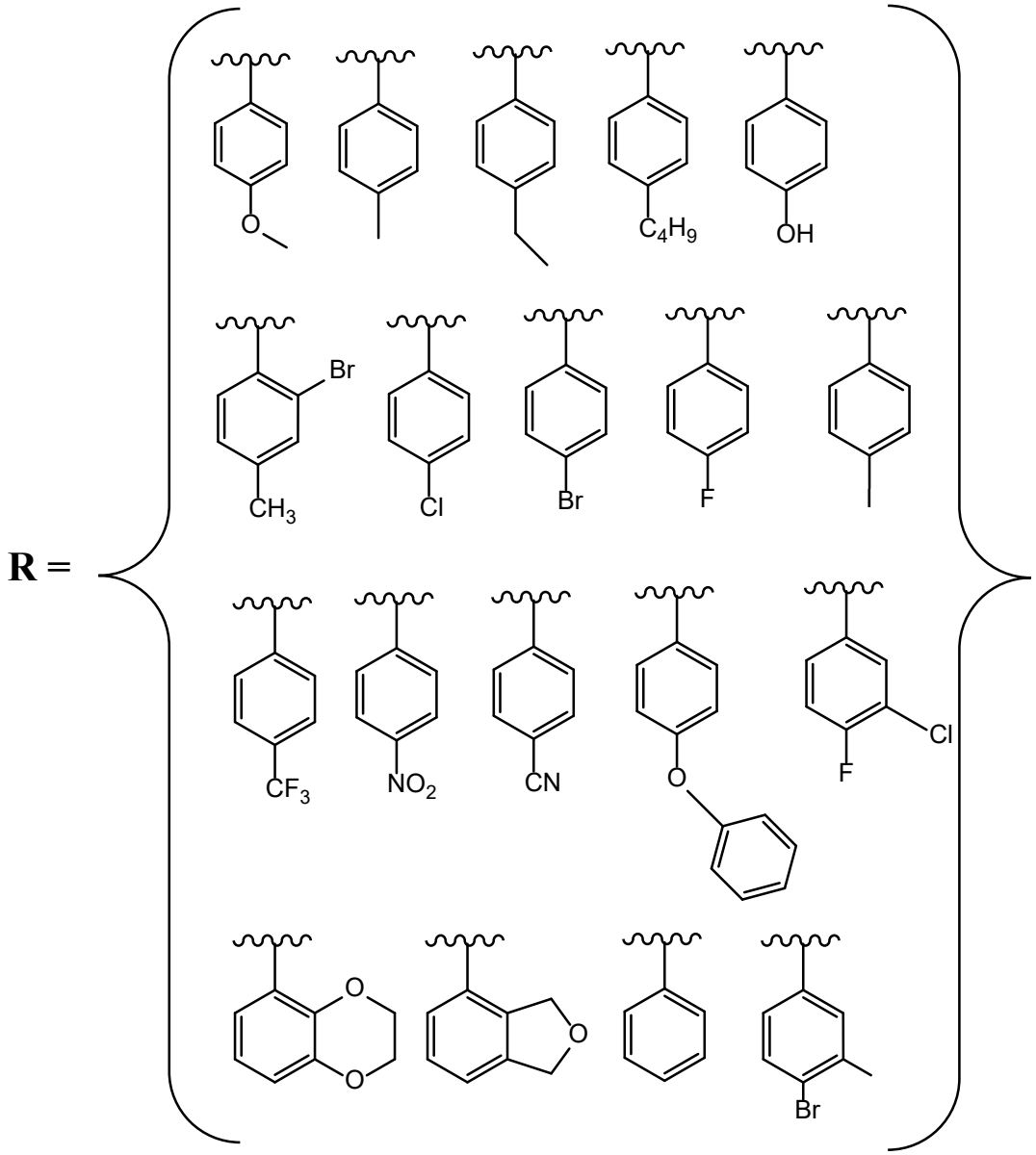

Scheme 3: General scheme for azide synthesis via anilines

5.2.2.3 General procedure for the synthesis of 1,2,3-triazoles

The substituted azides (1.5 eq.) were solubilized in a round bottom flask containing the solvent mixture H_2O (2 mL) and t-BuOH (2 mL). Then, alkyne, i.e., compound 2 (1.0 eq.), copper sulfate pentahydrate $CuSO_4.5H_2O$ (1 mol %), and sodium ascorbate (10 mol %) were added, respectively (Scheme 04). The mixture was left at room temperature and stirred for 12 h. After completion of the reaction, it was extracted with ethyl acetate (3 times). The combined organic layer was dried over anhydrous Na_2SO_4 and concentrated under reduced pressure on a

rotavapour to give the crude product, which was purified by column chromatography on silica gel using n-hexane: ethyl acetate (85:15 to 60:40 v/v) mixture as eluent to afford the desired pure products in 57-86% yields.

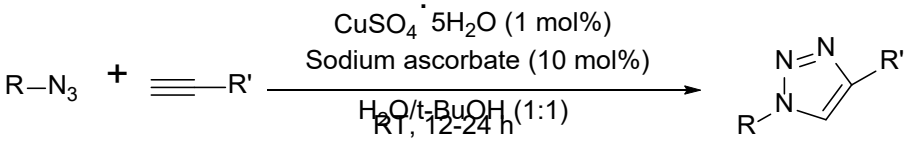

Scheme 04: General scheme for 1,2,3-triazole synthesis

5.2.3 *In silico* studies

5.2.3.1 Molecular docking studies on Erα

Molecular docking of MDL, 5-FU, Tamoxifen, and VNS-10 to ERα (PDB ID: 3ERT) was carried out by AutoDock Vina, in which the Iterated Local Search Globule Optimizer was applied as an optimization algorithm (146, 191). 2D structures of MDL, 5-FU, Tamoxifen and VNS-10 were prepared in ChemBioDraw Ultra 14.0 and minimized with the ChemBio3D Ultra 14.0. The receptor protein structures and ligand coordinates were prepared as follows: 1) the natural ligand and water molecules were removed from the crystal structure; 2) all hydrogen atoms were added to each protein and ligand to be docked, and each coordinate file of protein and ligand was generated as PDBQT file using AutoDockTools-1.5.6 (The Scripps Research Institute, La Jolla, California, USA); 3). A grid box for the binding site covered the catalytic site of the protein or 40 Å in the three dimensions for the allosteric binding site and centered at the geometric center of the protein.

The above prepared PDB files (proteins and ligands) were imported into the auto dock and saved into a pdbqt file format. Further, grid parameters were fixed by targeting amino acids from the active sites; Erα, and grid position was validated for Erα. Genetic Algorithms were set to 100 runs and docking parameters were marked as defaults followed by docking assigned

through Lamarckian genetic algorithm 4.2 (192). Further, ligands were docked against the target proteins (ERα). The resulting docking conformations were seen under the analysis window. These docking conformations (2D and 3D) were analyzed and documented using discovery studio visualizer 2021 client (193).

5.2.3.2 Molecular dynamic simulations of VNS-10

Molecular dynamics serves as a powerful tool for exploring the physical mobility and dynamic progression of protein-ligand complexes. So, to evaluate the stability of the docked molecules, the docked protein-ligand complex was simulated for 100 ns using GROMACS 2020 software (194). The binding interaction profile and stability of the docked ligands were analyzed on the ERα active site (PDB ID: 3ERT). The best-docked pose of the ligand was used to generate ligand topology files with the help of the CHARMM-GUI web server using the input generator for the GROMACS. The server utilizes the CHARMM 36 m force field to the ligand (195). The TIP3 model was used to solvate the protein, and the protein was neutralized using the Monte Carlo ion placing method, adding Na^+ and Cl^- ions. The temperature was kept constant at 303.15 K with a Noose Hoover thermostat. All the parameters, like NVT and NPT files, were generated. At last, the system was subjected to production simulation for 100 ns. When the MD run was completed, all the trajectories were analyzed using Gromacs utilities. Root means square deviation (RMSD), root mean square fluctuation (RMSF), number of hydrogen bonds, and radiation of gyration (RoG) were analyzed and plotted.

5.2.3.3 Drug-likeness, ADME, and toxicity predictions

The drug-likeness, ADME, and toxicity properties of all synthesized compounds were predicted using online software tools swissADME (http://www.swissadme.ch/) (196).

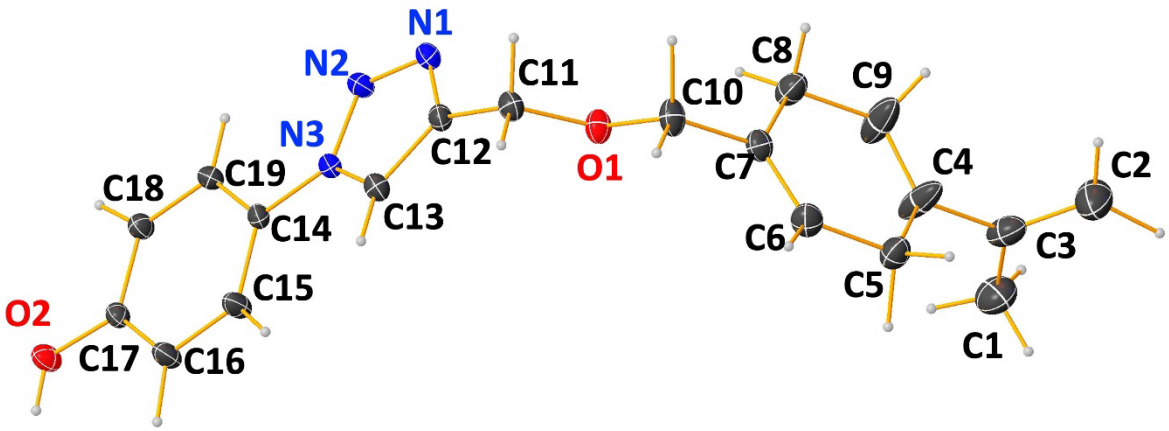

Figure 43 ORTEP diagram of compound VNS08 (40% ellipsoid plot)

5.5. Biological experiments

5.5.1. Cell lines, cell culture, growth conditions and reagents

A panel of human cancer cell lines namely MCF-7 (Breast), MDA-MB-231 (Breast), A549 (Lungs), SiHa (Cervical), BL60 (Melanoma), and normal kidney cell line (HEK-293) were purchased from National Centre for Cell Science (NCCS), Pune, India for screening of VNS01-VNS23 synthesized potential anticancer test molecules. The cell lines were grown in T75 tissue culture flasks in complete growth medium (DMEM) added with 10% FBS, 100 µg/mL streptomycin as well as 100 units/mL penicillin in humidified carbon dioxide incubator (New Brunswick, Galaxy 170R, Eppendorf) at 37 ºC, 5% CO_2 with 95% relative humidity. Acridine orange, Ethidium bromide, Propidium iodide, DCFDA (2′, 7′-dichlorofluorescein diacetate) were procured from Sigma-Aldrich (St. Louis, MO, USA). MTT dye was purchased from Hi Media, India. Monolayer cultures of the above cell lines were trypsinized using 0.25% trypsin/EDTA (1 mM) solution. After the cells detached, the trypsin/EDTA solution activity was stopped using a complete growth medium and centrifuged at 1000 rpm for 5 min. Cells were again dispersed in a complete growth medium in tissue culture flasks and incubated in a CO_2 incubator. When cells attained approx. 50-60%

confluency, they were treated with target compounds dissolved in DMSO and the untreated control cultures with (DMSO, < 0.2%).

5.5.2. *In vitro* cytotoxicity assay

5.5.2. Cytotoxicity activity against different cancer cell lines

To determine the antiproliferative effect of synthesized compounds on MCF-7 (Breast), MDA-MB-231 (Breast), A549 (Lungs), SiHa (Cervical), BL60 (Melanoma), and a normal kidney cell (HEK-293), compounds VNS01-VNS23 were tested by the MTT assay on these cell lines. Briefly, 100 µL/well of cell suspensions were seeded at the density of 1×10^4 viable cells per well in a 96-well plate in DMEM and kept for 24 h of incubation at 37 ºC and 5% CO_2. When cells attained 50-60% confluency, they were treated with various concentrations of test compounds and incubated for another 48 h. Tamoxifen citrate and 5 FU were used as standard drugs for reference.

Cell viability was determined by adding 100 µl of 3-(4,5-Dimethyl-2-thiazolyl)-2,5-diphenyl-2H-tetrazolium bromide, MTT reagent (0.5 mg/ml) dissolved in serum-free media added to each well and incubated for 4 h. Then, the old medium was discarded, and the crystals were dissolved in 200 µL of DMSO, and the absorbance of each well was taken at 570 nm in a multimode plate reader.

Cell viability was measured as the percentage absorbance compared to the control (nontreated cells). The graph was plotted between different concentrations and percentage inhibition. All the values were expressed as Mean ± SEM in three different experiments in which each treatment was performed in triplicates. Percent cell viability and percent inhibition were calculated using the following formula and were tested at least in triplicates.

$$Cell\ viability\ (\%) = \frac{Absorbance\ of\ sample}{Absorbance\ of\ control} \times 100$$

4.5.4. Acridine orange/ethidium bromide staining

In order to examine apoptotic cell death qualitatively, morphological variations in cell structure were detected using AO/EB staining. Briefly, cells were seeded at a density of 1×10^5 cells per well in 12 well tissue culture plates supplemented with 10% FBS, and after 24 h of incubation at 37 ºC and 5% CO_2, they were treated with 1.5 µM, 3 µM and 10 µM concentration of the compounds VNS10 and VNS15 dissolved in the culture media. After 48 h of incubation, the cells were washed twice with PBS, and cells were fixed with 4% PFA (paraformaldehyde) stained with acridine orange and ethidium bromide (AO/EB) at a concentration of 5 µg/ml for 5 min and incubated at 37 ºC for 20 min. The cells were then washed with PBS, and the images were taken in an inverted fluorescence microscope (EVOS FLC Invitrogen fluorescence microscope, Life technologies) to observe the morphological features of the cells with excitation (488 nm) and emission (550 nm) and 200x magnification.

4.5.5. Reactive oxygen species (ROS) generation assay

Dye 2′,7′-dichlorofluorescein diacetate (DCFH-DA) was used to measure intracellular ROS production. DCFH gets transformed into highly fluorescent 2′, 7′-dichlorofluorescein (DCF) in the presence of an oxidant. In this study, MCF-7 cells in the density of 1×10^5 cells were seeded into six-well plates and then incubated at 37 ºC overnight in 5% CO_2. After incubation, cells were treated with compounds including VNS10 and VNS15 for another 24 h, respectively. After 24 h co-incubation, the cells were washed with cold PBS, fixed with 70% ethanol, and incubated at 4 °C for 4 h. The collected cells were stained with 2,7-dichlorodi-hydrofluorescein diacetate (DCFH-DA) (10 µM) and further incubated in the dark for 30 min. Thereafter, the cells were washed twice with PBS and observed under an inverted fluorescence microscope (EVOS FLC Invitrogen fluorescence microscope, Life Technologies).

4.5.6. Cell apoptosis assay

Detection of apoptosis of MCF-7 cells caused by compound VNS10 was made through the annexin V- Alexa Fluor apoptosis detection kit according to the manufacturer's protocol. MCF-7 cells were seeded into a 6-well culture plate (at a density of 5×10^5 cells/well) and cultured for 24 h. After that, cells were treated with compound VNS10 at certain concentrations (1.5, 3, and 6.0 μM) for 24 h. After incubation 48 h, cells were trypsinized, washed with ice PBS, suspended into 1 x binding buffer, and doubled stained with annexin V- Alexa Fluor and PI for 30 min, and cell apoptosis results were recorded and analyzed by flow cytometry (BD FACS Calibur, USA).

4.2.4. Cell cycle analysis

MCF-7 cells were seeded into a 6-well culture plate (5×10^5 cells/well) and cultured for 24 h. After that, DMSO was used as a blank control, and cells were incubated with compound VNS10 at the specified concentration (1.5, 3, and 6.0 μM) for 48 h. Then, the suspended and adherent cells were collected and washed with PBS. All the cells were fixed with ice-cold ethanol (70 %) at -20 ºC overnight. Centrifugation was carried out at 2000 rpm for 5 min to remove the supernatant, and washed with ice PBS, cells were preincubated with RNase A (100 μg/mL) at 37 ˚C for 30 min. After that, cells were collected and stained with 1 mg/mL of PI in the dark for 30 min, respectively. Thereafter, the cell samples were analyzed by the flow cytometer (BD FACS Calibur, USA) for cell cycle distribution.

4.2.8. Statistical analysis

The results are interpreted as mean ± SD belonging to three independent tests. Standard deviations were calculated using Graph Pad Prism 6.0 (Graph Pad Software Inc., San Diego, CA, USA).

5.3 Results and Discussion

Preparation of 1,2,3-triazole derivatives was undertaken and click chemistry strategy was adopted on the MDL or PLA (prepared as per Scheme 1) and made to react with appropriate azides (prepared as per Scheme 2 and 3). A library of around twenty-three triazole derivatives bearing structural diversity was thus prepared, and their chemical identity was established by spectral analysis. The overall chemical yields of the synthesized compounds ranged from 92 to 98%.

Azides used in click reactions were synthesized in a few steps from simple precursors following known reaction procedures. All triazole derivatives were purified through silica gel column chromatography and were fully characterized by IR, NMR, and high-resolution mass spectral (HRMS) analysis. In ^{1}H NMR spectra, the characteristic signal for hydrogen present in the triazolic ring was observed within the δ 7.89-8.31 ppm range in all the products, and carbon chemical shifts were also compatible with the structures of target compounds.

5.3.1 Characterization of synthesized 1,2,3-triazole derivatives

a.) Structural identification of compound VNS01

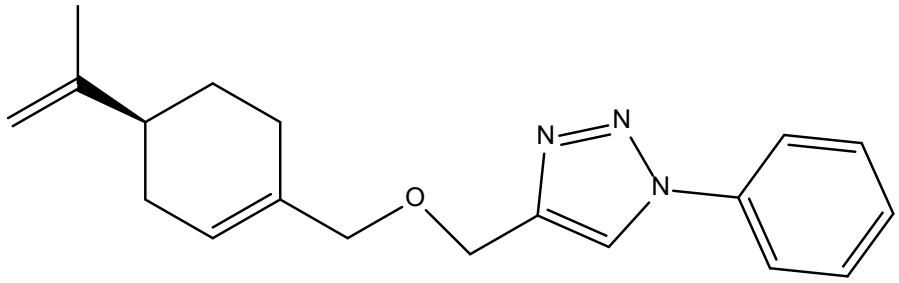

^{1}H NMR (500 MHz, $CDCl_3$) δ 8.00 (s, 1H), 7.75 – 7.69 (m, 2H), 7.53 – 7.47 (m, 2H), 7.45 – 7.39 (m, 1H), 5.77 (s, 1H), 4.73 – 4.69 (m, 2H), 4.68 – 4.64 (m, 2H), 3.99 (s, 2H), 2.20 – 2.08 (m, 4H), 1.97 (t, *J* = 14.7 Hz, 1H), 1.84 (ddd, *J* = 9.9, 4.6, 2.3 Hz, 1H), 1.73 (s, 3H), 1.53 – 1.42 (m, 1H). ^{13}C NMR (125 MHz, $CDCl_3$) δ 149.74, 146.27, 137.06, 134.17, 129.75 (2C), 128.74, 125.29, 120.65, 120.53, 108.70, 75.04, 63.14, 41.02, 30.51, 27.43, 26.42, 20.78.
ESI-HRMS calculated for $C_{19}H_{23}N_3O$ $[M+H]^+$: 352.2311, found 352.2336.

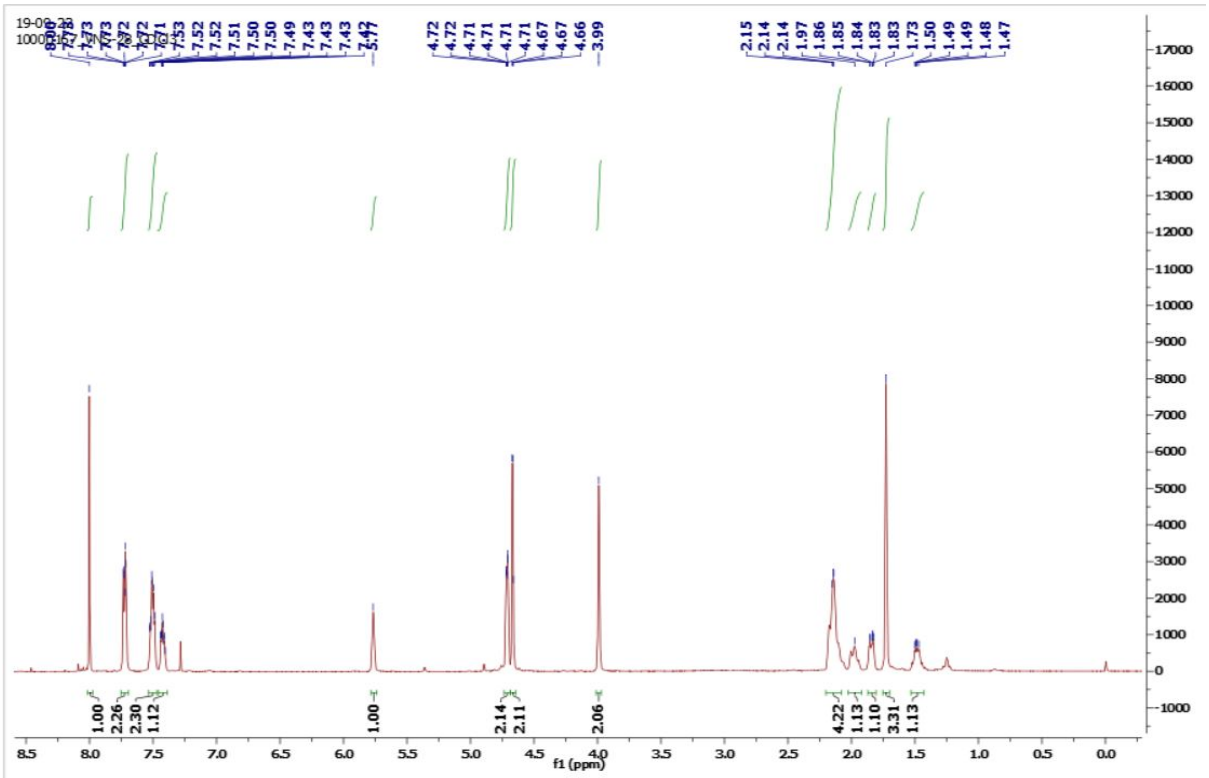

Figure 44 ^{1}H NMR Spectra of compound-VNS01

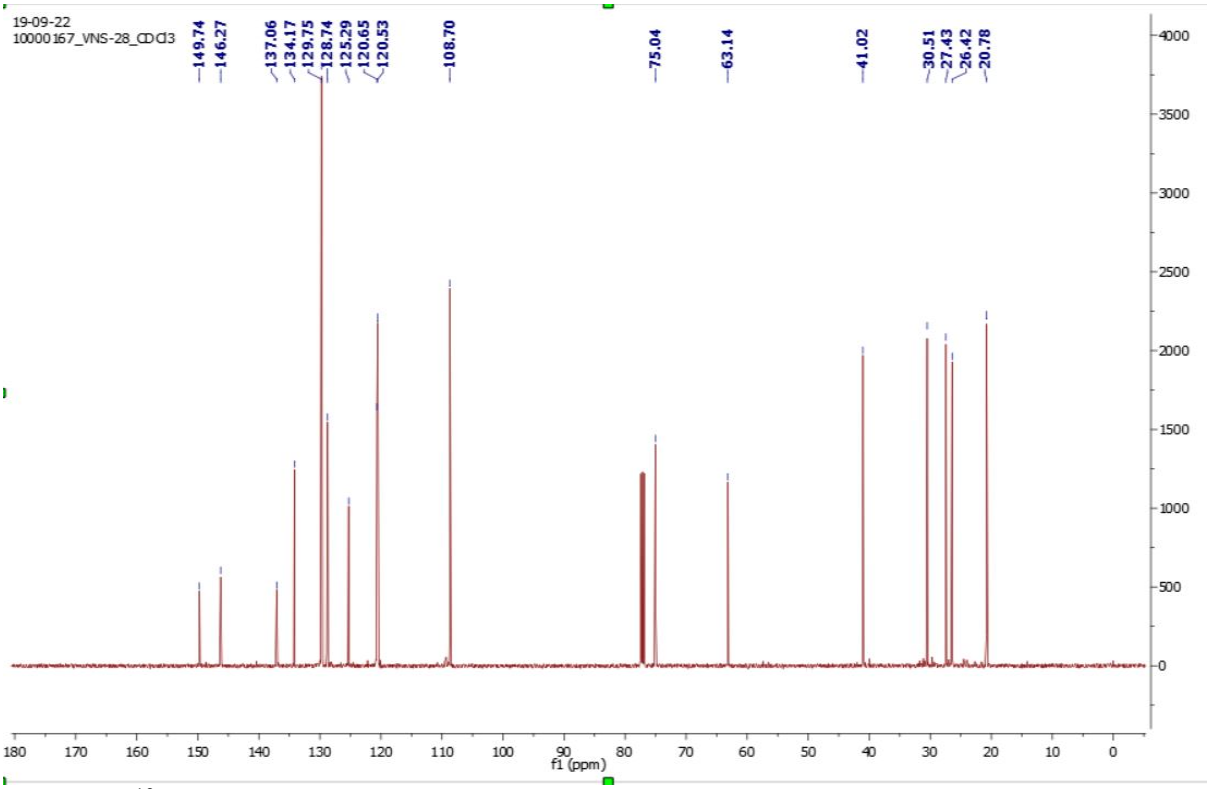

Figure 45 ^{13}C NMR Spectra of compound-VNS01

b.) Structural identification of compound VNS02

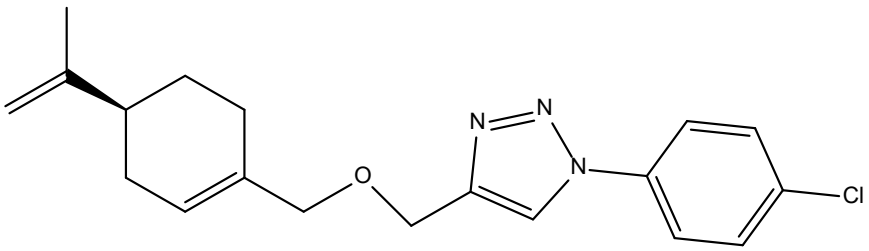

^{1}H NMR (500 MHz, $CDCl_3$) δ 7.98 (s, 1H), 7.70 (d, J = 8.7 Hz, 2H), 7.53 – 7.49 (m, 2H), 5.79 (s, 1H), 4.73 (s, 2H), 4.68 (s, 2H), 4.01 (s, 2H), 2.23 – 2.08 (m, 4H), 2.00 (s, 1H), 1.89 – 1.83 (m, 1H), 1.75 (s, 3H), 1.55 – 1.45 (m, 1H). ^{13}C NMR (125 MHz, $CDCl_3$) δ 149.74, 146.63, 135.57, 134.52, 134.13, 129.95 (2C), 125.39, 121.69 (2C), 120.46, 108.71, 75.14, 63.14, 41.03, 30.52, 27.43, 26.43, 20.78. ESI-HRMS calculated for $C_{19}H_{22}ClN_3O$ $[M+H]^+$: 344.1451, found 344.1472.

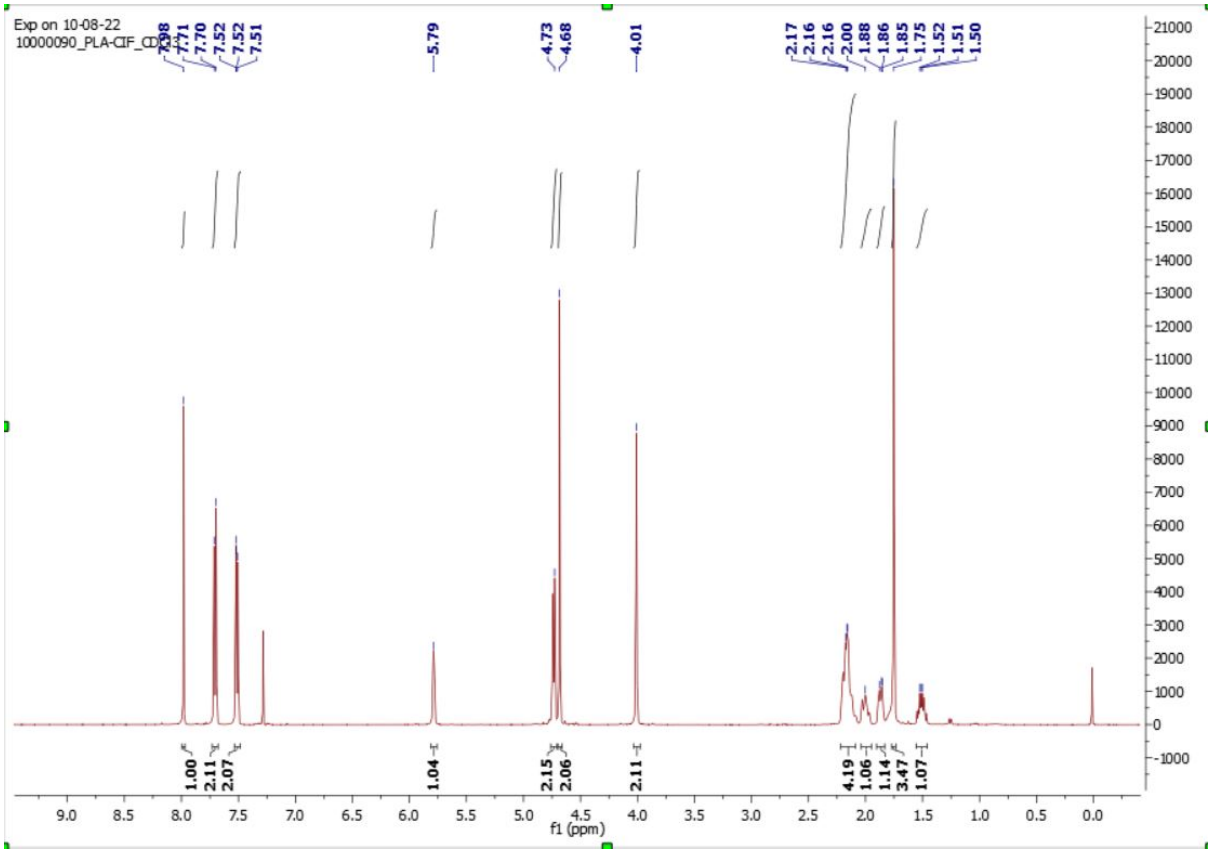

Figure 46 ^{1}H NMR Spectra of compound- VNS02

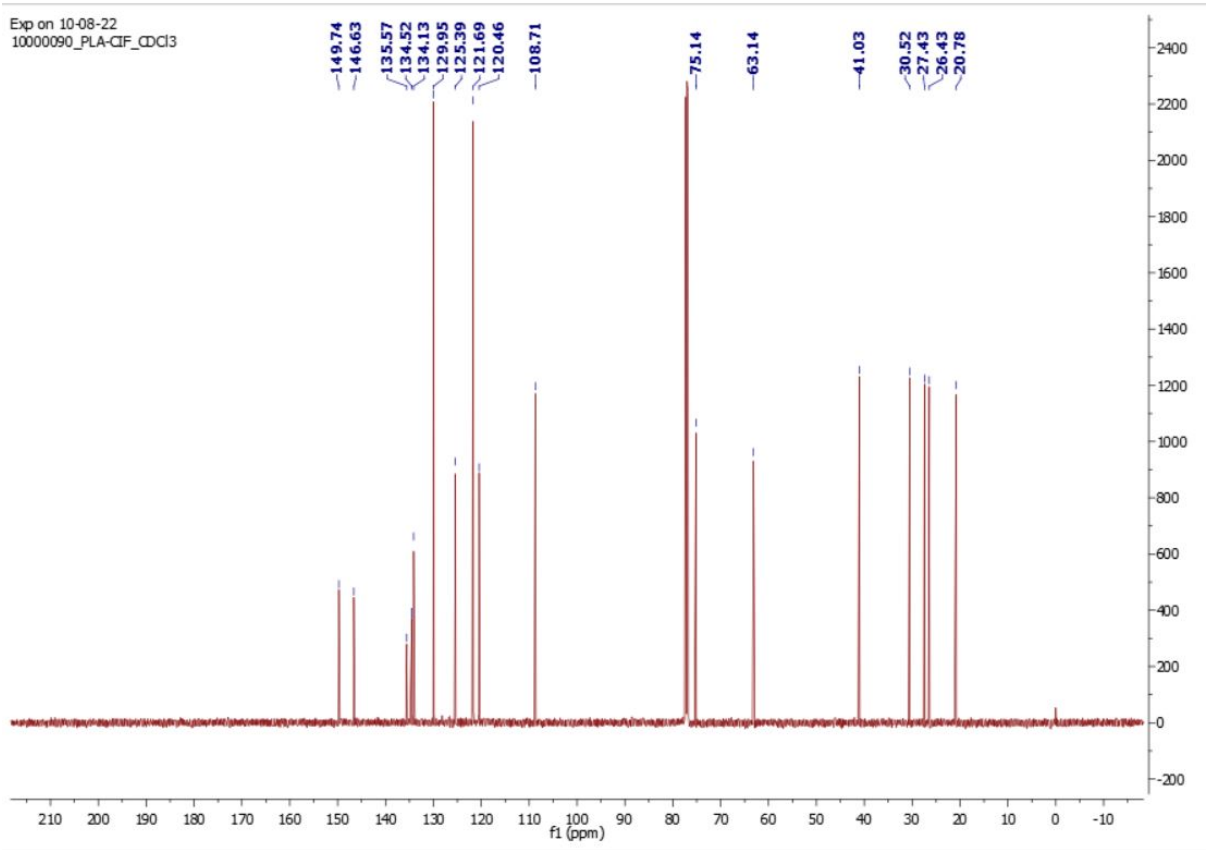

Figure 47 ^{13}C NMR Spectra of compound-VNS02

c.) Structural identification of compound VNS05

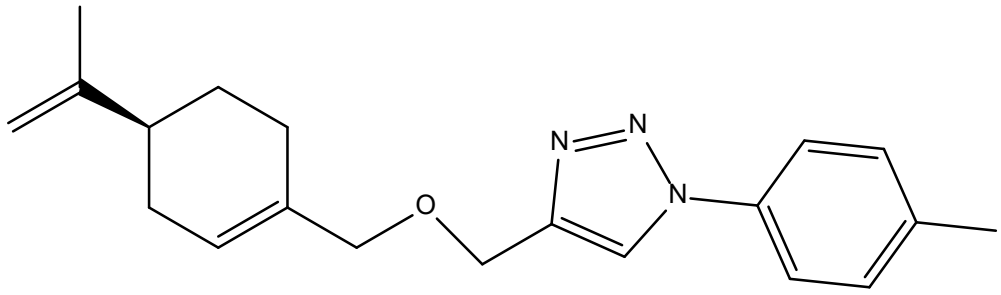

^{1}H NMR (500 MHz, $CDCl_3$) δ 7.96 (s, 1H), 7.65 – 7.59 (m, 2H), 7.33 (dd, J = 8.5, 0.5 Hz, 2H), 5.79 (s, 1H), 4.74 (d, 2H), 4.69 (s, 2H), 4.01 (s, 2H), 2.44 (s, 3H), 2.22 – 2.11 (m, 4H), 2.05 – 1.95 (m, 1H), 1.90 – 1.84 (m, 1H), 1.76 (s, 3H), 1.56 – 1.46 (m, 1H). ^{13}C NMR (126 MHz, $CDCl_3$) δ 149.81, 146.16, 138.85, 134.84, 134.22, 130.25(2C), 125.28, 120.60, 120.49(2C), 108.68, 75.05, 63.24, 41.06, 30.53, 27.45, 26.45, 21.11, 20.79. ESI-HRMS calculated for $C_{20}H_{25}N_3O$ $[M+H]^+$: 324.2071, found 324.2054.

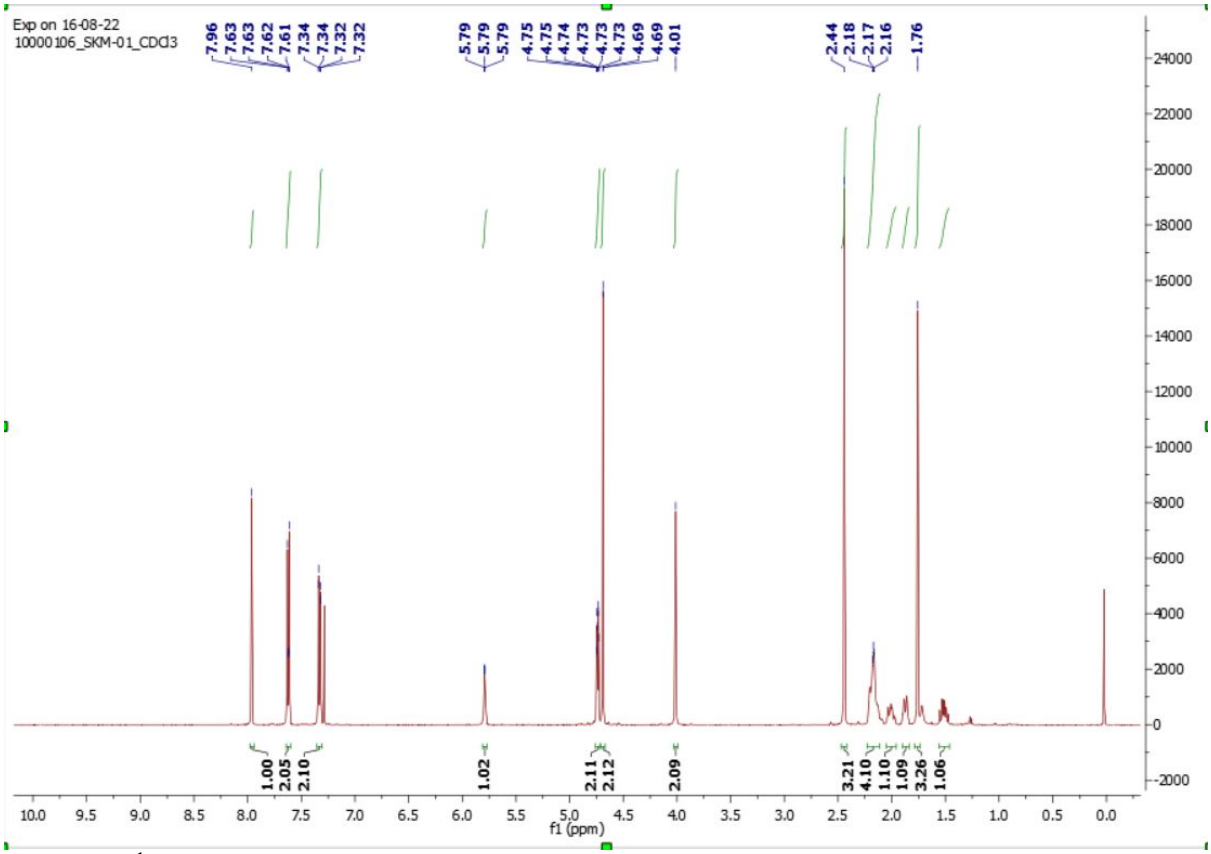

Figure 48 ^{1}H NMR Spectra of compound-VNS05

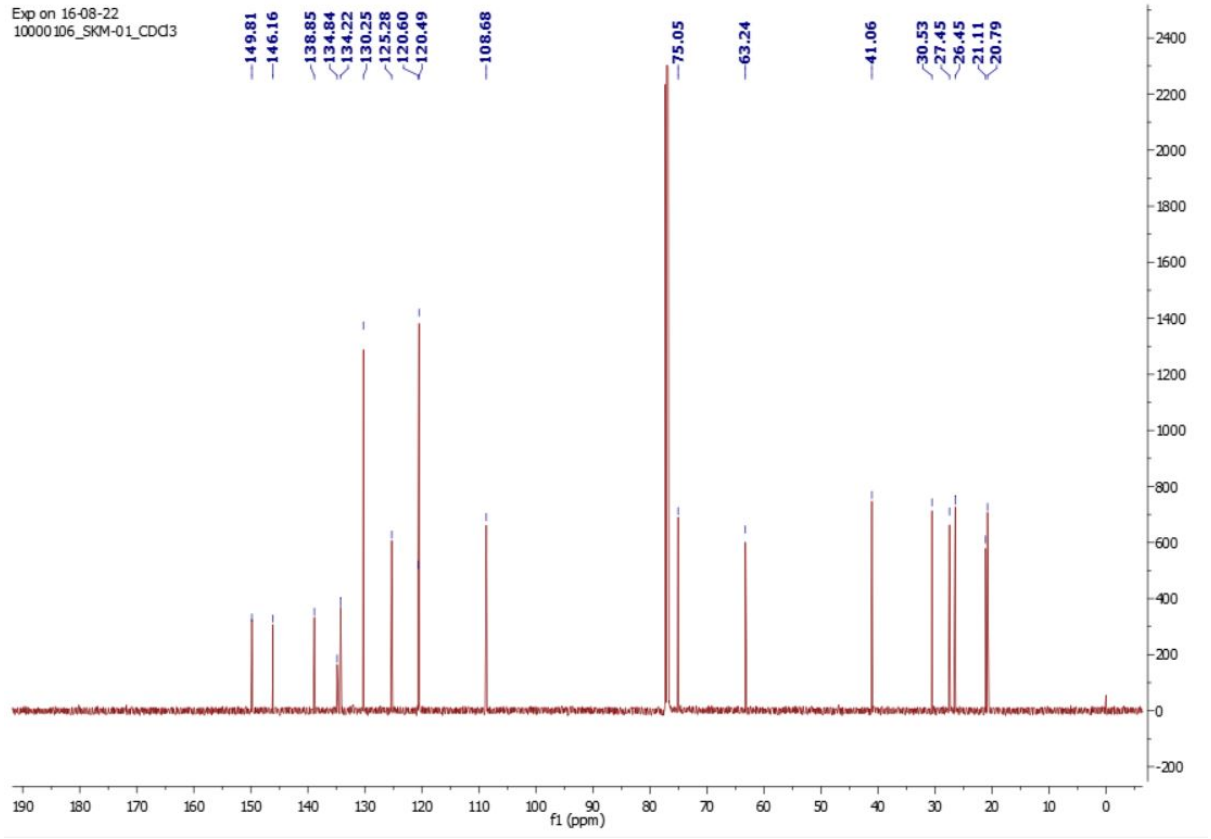

Figure 49 ^{13}C NMR Spectra of compound-VNS05

d.) Structural identification of compound VNS08

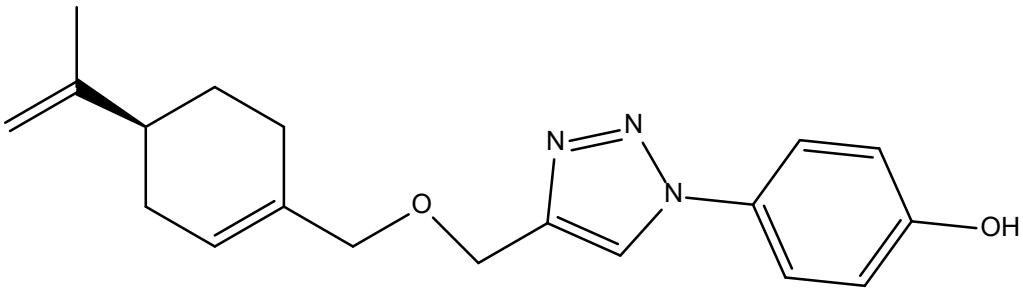

^{1}H NMR (500 MHz, $CDCl_3$) δ 7.92 (s, 1H), 7.59 – 7.51 (m, 2H), 7.08 – 7.02 (m, 2H), 5.79 (s, 1H), 4.73 (dd, *J* = 7.7, 1.1 Hz, 2H), 4.69 (s, 2H), 4.02 (s, 2H), 2.16 (s, 3H), 2.04 – 1.95 (m, 1H), 1.89 – 1.84 (m, 1H), 1.75 (s, 3H), 1.55 – 1.45 (m, 1H). ^{13}C NMR (125 MHz, $CDCl_3$) δ 157.27, 149.75, 145.77, 134.02, 129.86, 125.62, 122.46 (2C), 121.17, 116.56 (2C), 108.71, 75.18, 62.92, 41.00, 30.51, 27.41, 26.42, 20.79. ESI-HRMS calculated for $C_{19}H_{23}N_3O_2$ $[M+H]^+$: 326.1863, found 326.1823

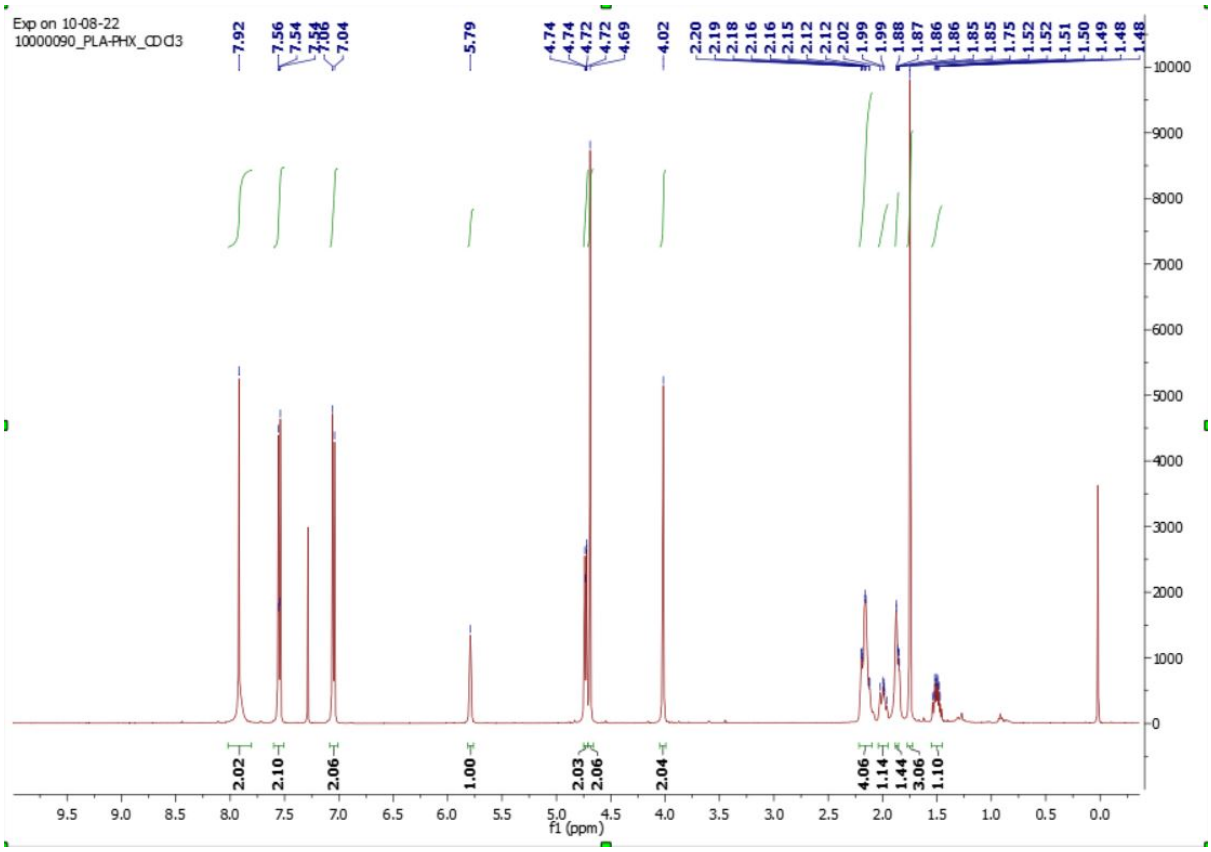

Figure 50 ^{1}H NMR Spectra of compound-VNS08

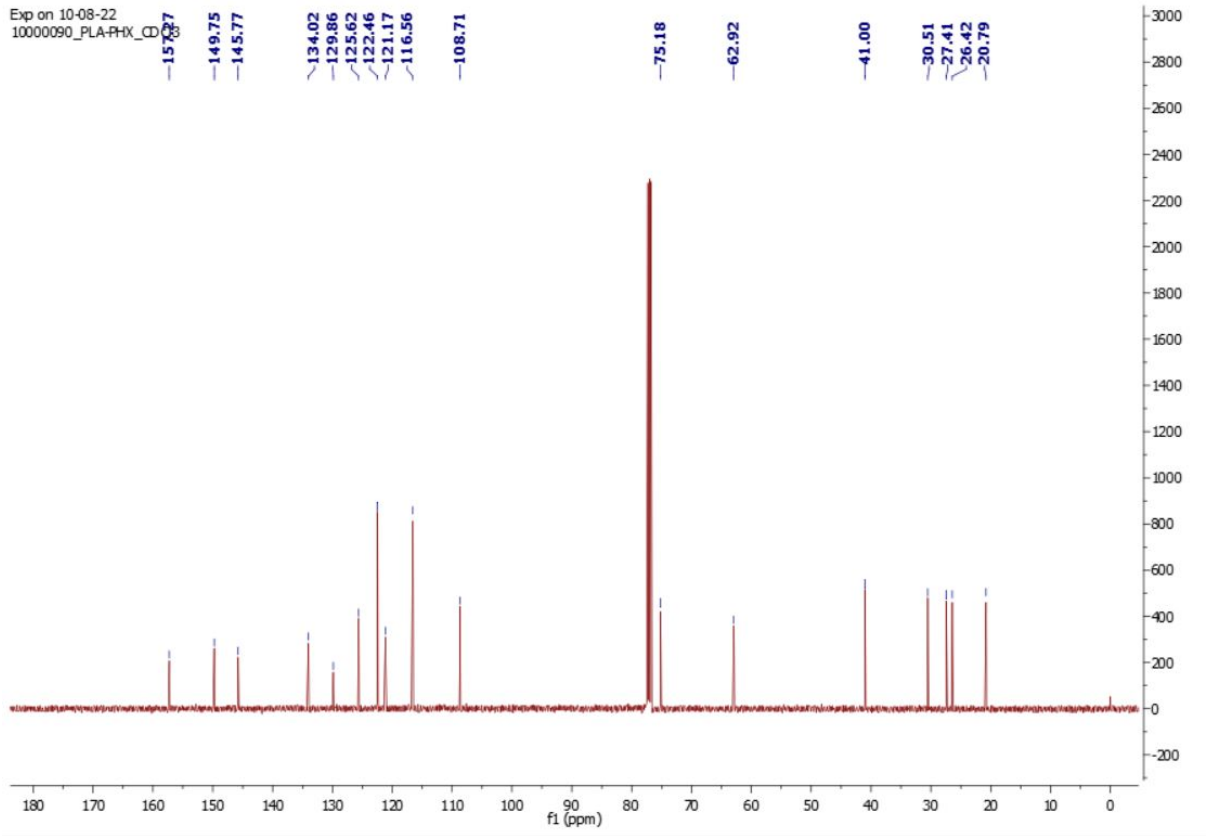

Figure 51 ^{13}C NMR Spectra of compound-VNS08

e.) Structural identification of compound VNS09

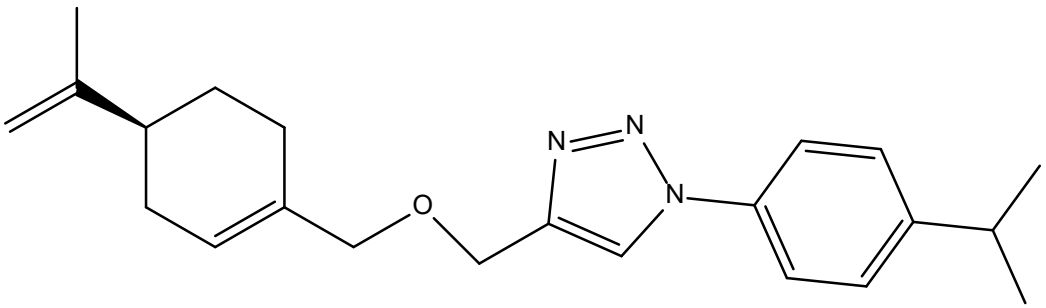

^{1}H NMR (500 MHz, $CDCl_3$) δ 7.97 (s, 1H), 7.66 (d, J = 10.1 Hz, 2H), 7.38 (d, J = 8.3 Hz, 2H), 5.78 (s, 1H), 4.73 (d, 2H), 4.68 (s, 2H), 4.01 (s, 2H), 3.02 – 2.96 (m, J = 13.8, 6.9 Hz, 1H), 2.15 (d, 4H), 2.04 – 1.95 (m, J = 16.2, 13.8 Hz, 1H), 1.90 – 1.83 (m, 1H), 1.75 (s, 3H), 1.50 (ddd, J = 23.6, 11.5, 6.0 Hz, 1H), 1.30 (d, J = 6.9 Hz, 6H). ^{13}C NMR (125 MHz, $CDCl_3$) δ 149.86, 146.19, 135.09, 134.30, 127.76, 125.36, 120.70, 108.77, 75.12, 63.31, 41.13, 33.91, 30.60, 27.53, 26.52, 23.98, 20.86. ESI-HRMS calculated for $C_{22}H_{29}N_3O$ $[M+H]^+$: 352.2384, found 352.2362.

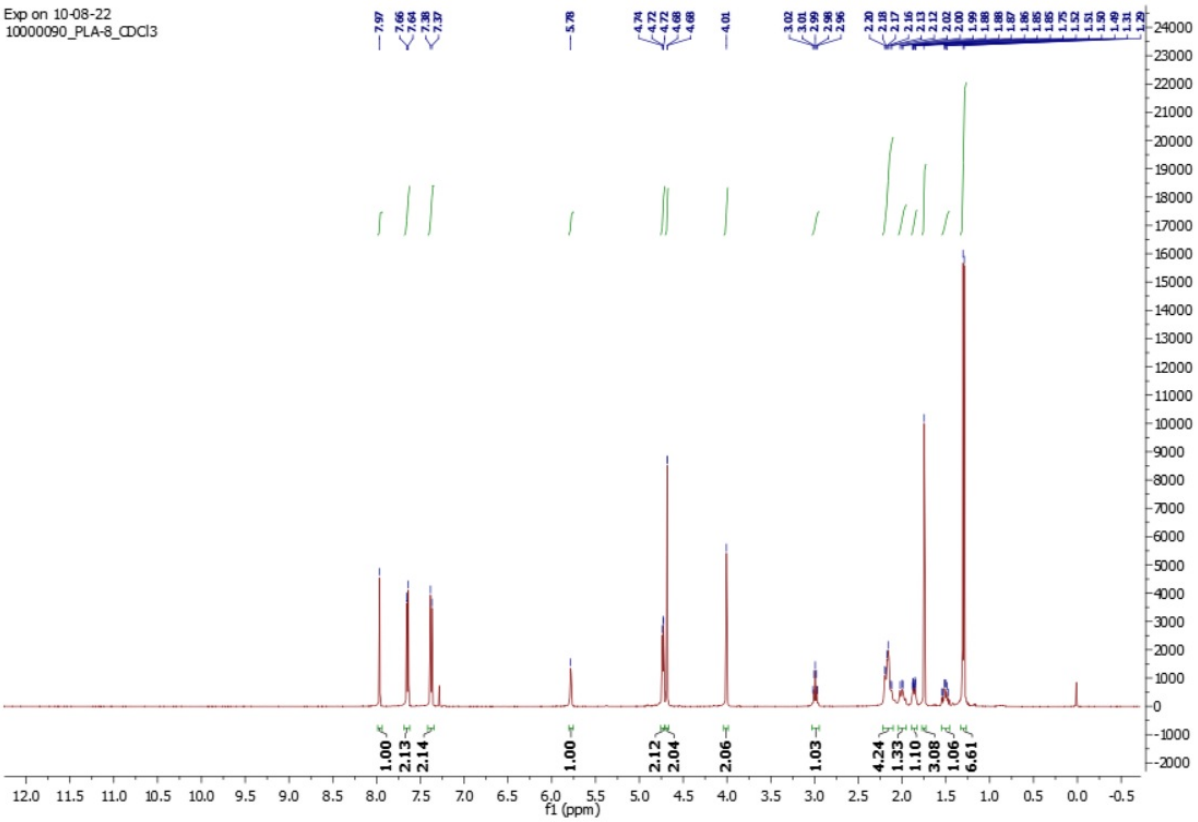

Figure 52 ^{1}H NMR Spectra of compound-VNS09

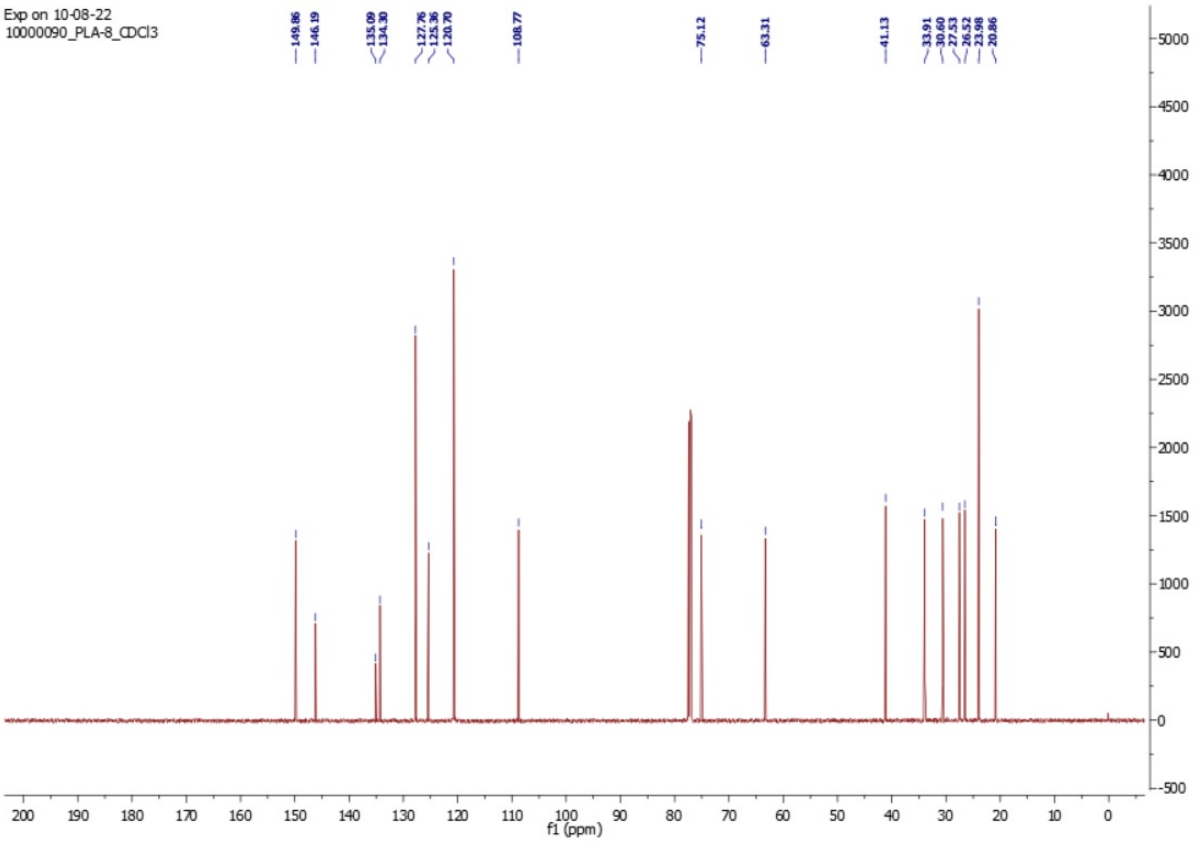

Figure 53 ^{13}C NMR Spectra of compound-VNS09

f.) Structural identification of compound VNS11

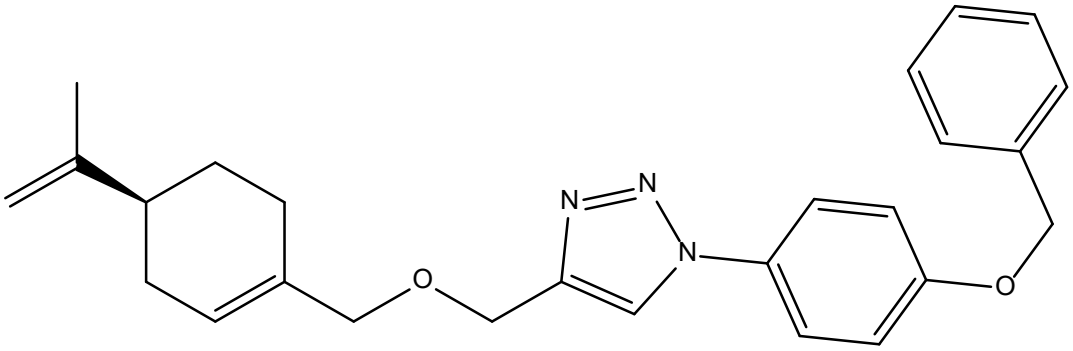

^{1}H NMR (500 MHz, $CDCl_3$) δ 7.91 (s, 1H), 7.64 (d, *J* = 8.8 Hz, 2H), 7.50 – 7.40 (m, 4H), 7.37 (t, *J* = 7.1 Hz, 1H), 7.11 (d, *J* = 8.8 Hz, 2H), 5.79 (s, 1H), 5.15 (s, 2H), 4.74 (d, *J* = 6.7 Hz, 2H), 4.69 (s, 2H), 4.01 (s, 2H), 2.23 – 2.11 (m, 4H), 2.05 – 1.96 (m, 1H), 1.88 (d, *J* = 12.7, 2.5 Hz, 1H), 1.76 (s, 3H), 1.56 – 1.46 (m, *J* = 23.5, 11.5, 6.0 Hz, 1H). ^{13}C NMR (125 MHz, $CDCl_3$) δ 159.07, 149.94, 146.24, 136.45, 134.34, 130.89, 128.85, 128.37, 127.61, 125.41, 122.36, 120.89, 115.88, 108.81, 75.17, 70.53, 63.37, 41.18, 30.65, 27.58, 26.57, 20.91. ESI-HRMS calculated for $C_{26}H_{29}N_3O_2$ $[M+H]^+$: 416.2333, found 416.2331.

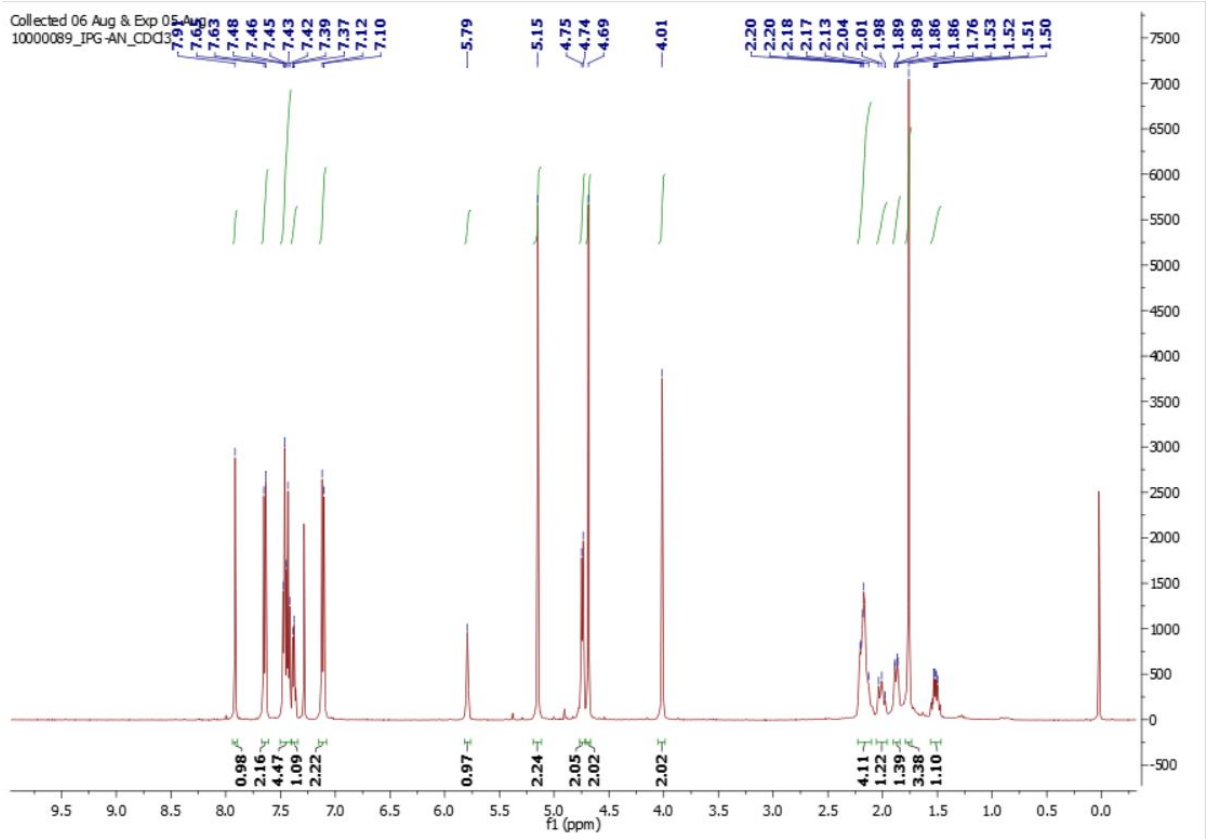

Figure 54 ^{1}H NMR Spectra of compound-VNS11

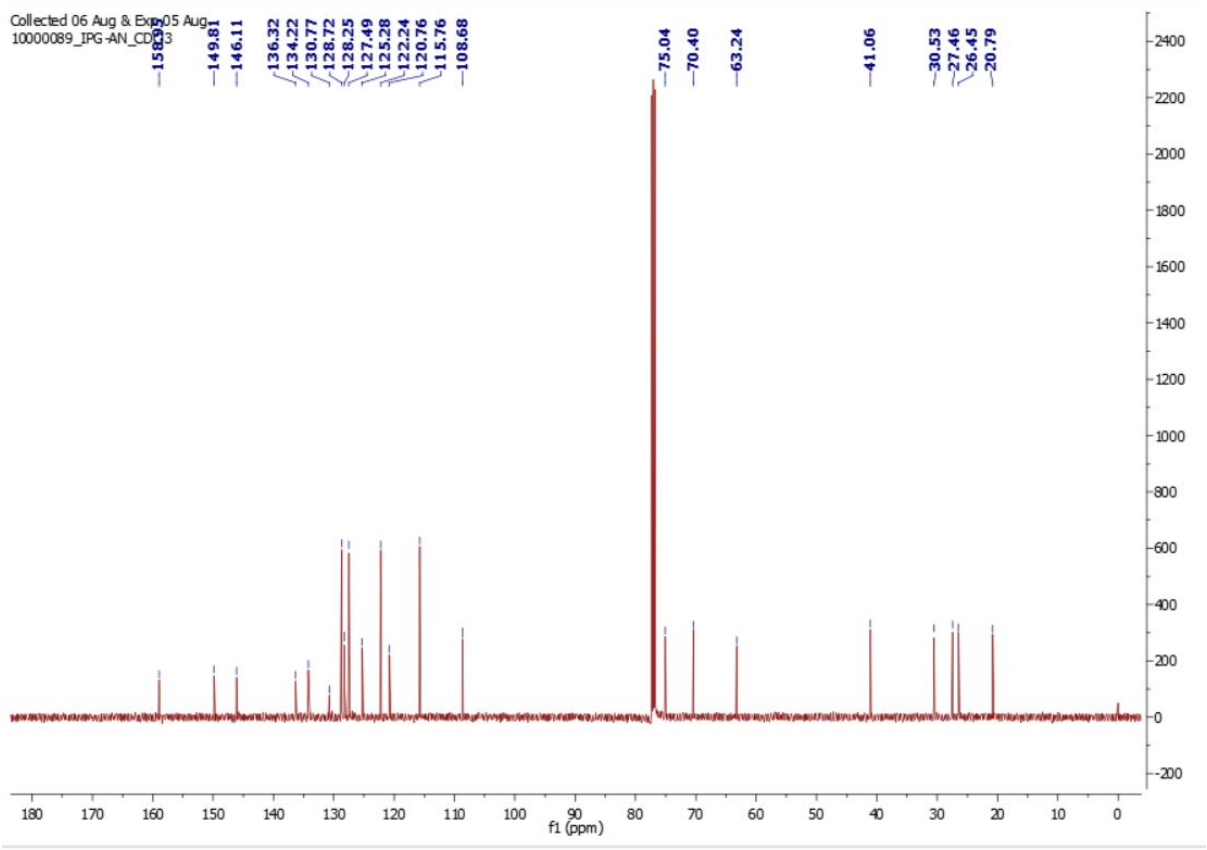

Figure 55 ^{13}C NMR Spectra of compound-VNS11

g.) Structural identification of compound VNS16

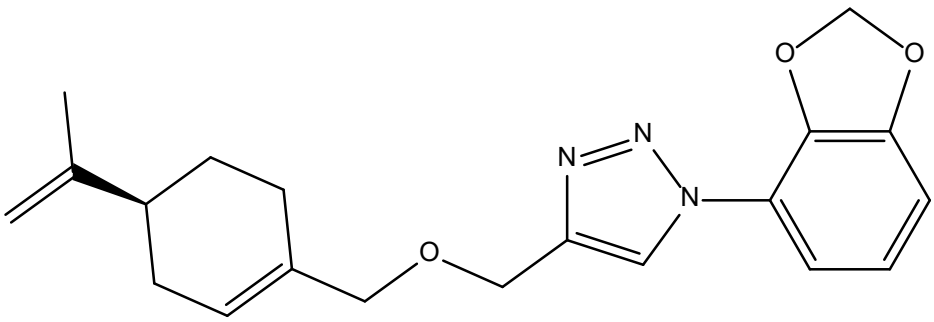

^{1}H NMR (500 MHz, $CDCl_3$) δ 7.89 (s, 1H), 7.26 (d, J = 2.1 Hz, 1H), 7.15 (dd, J = 8.3, 2.2 Hz, 1H), 6.92 (d, J = 8.3 Hz, 1H), 6.09 (s, 2H), 5.79 (s, 1H), 4.74 (d, 2H), 4.68 (s, 2H), 4.01 (s, 2H), 2.17 (ddd, J = 22.4, 12.6, 2.4 Hz, 4H), 2.05 – 1.96 (m, 1H), 1.90 – 1.84 (m, 1H), 1.76 (s, 3H), 1.56 – 1.46 (m, 1H). ^{13}C NMR (125 MHz, $CDCl_3$) δ 149.93, 148.75, 148.14, 146.26, 134.32, 131.75, 125.45, 121.03, 114.39, 108.81, 108.64, 102.95, 102.24, 75.21, 63.33, 41.18, 30.65, 27.58, 26.57, 20.92. ESI-HRMS calculated for $C_{20}H_{23}N_3O_3$ $[M+H]^+$: 354.1812, found 354.1791.

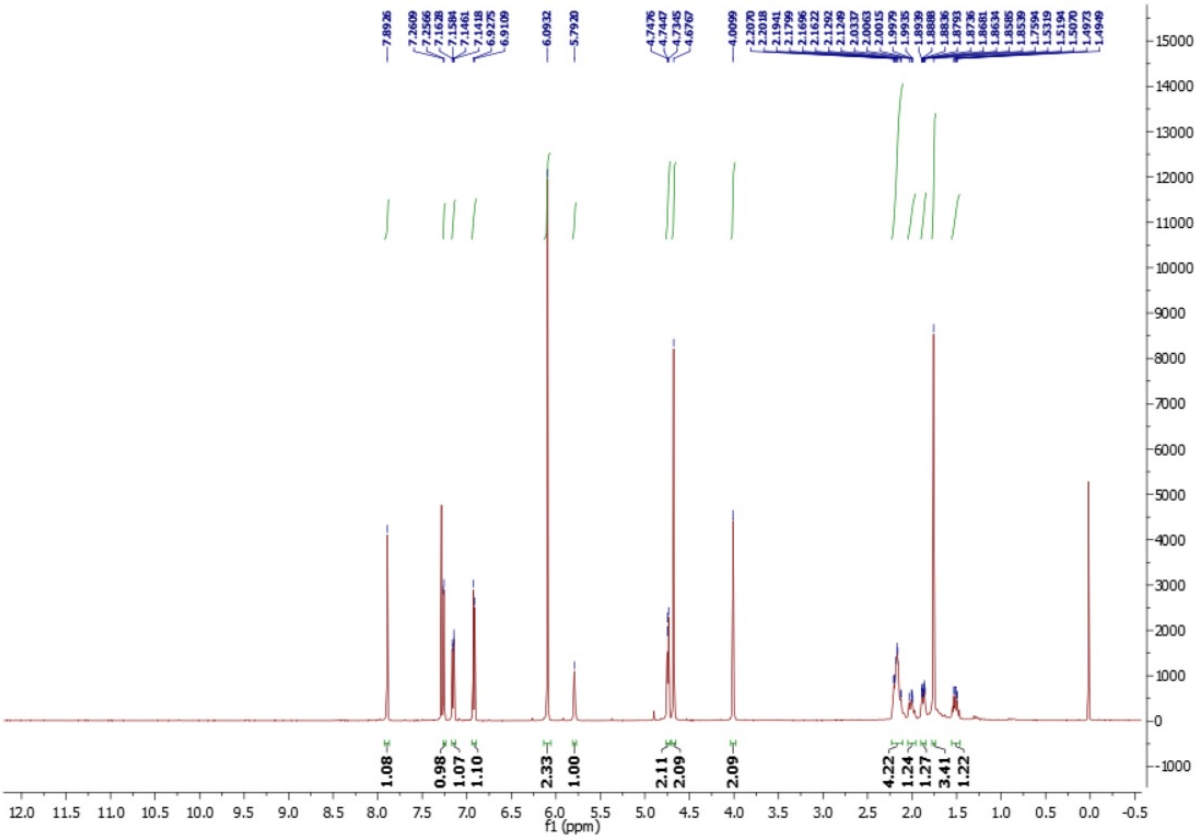

Figure 56 ^{1}H NMR Spectra of compound-VNS16

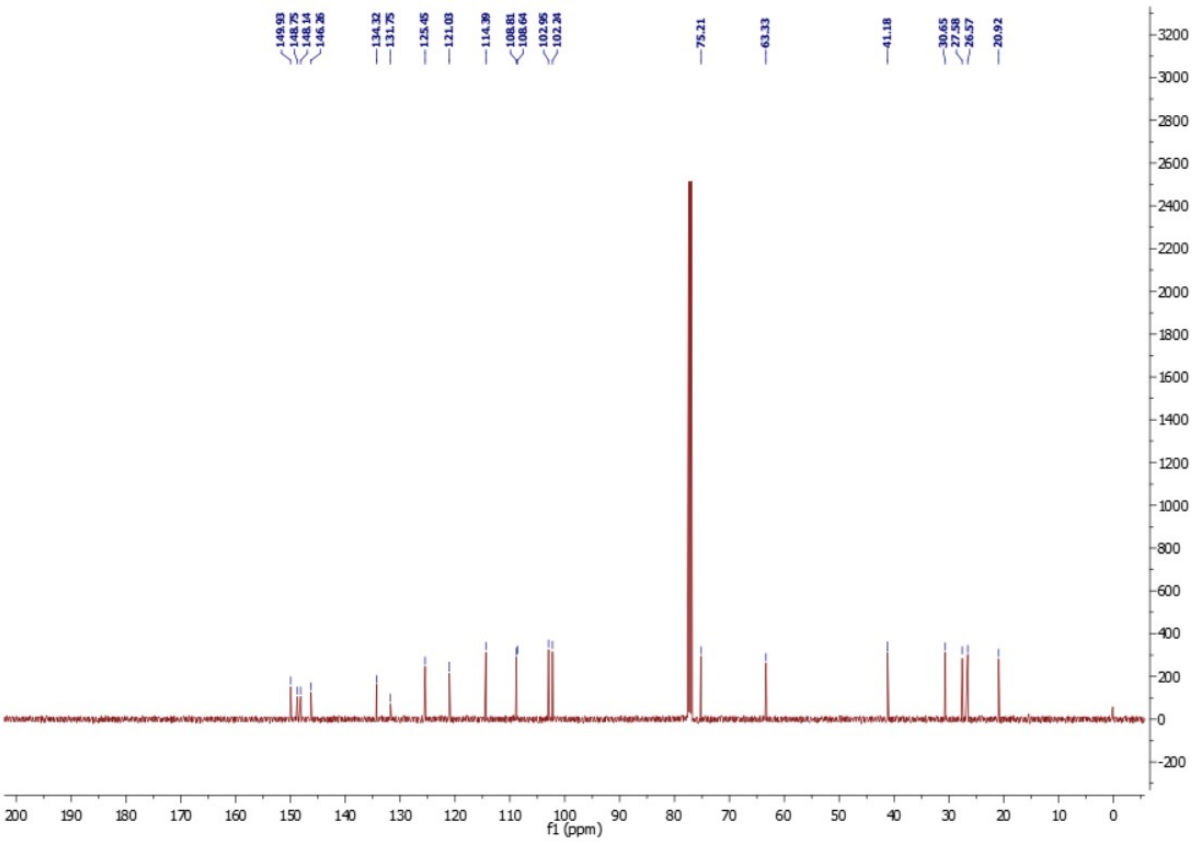

Figure 57 ^{13}C NMR Spectra of compound-VNS16

5.3.2 *In silico* studies

5.3.2.1 Molecular docking studies on estrogen receptor α (ERα)

The structure of the human estrogen receptor alpha ligand-binding domain in complex with 4-hydroxytamoxifen (PDB ID: 3ERT, resolution 1.9 Å) was obtained from the protein data bank; the raw structure was refined and utilized for this study. The docking studies were performed on all synthesized compounds within the active site of estrogen receptor α (ERα). The compounds showed binding energies between - 8.158 and - 10.001 kcal/mol and formed interactions with surrounding amino acid residues at active sites, such as ASP351, ALA350, TRP383, THR347, LEU525, MET343, MET421, GLU419, GLY420, ILE424, HIS524, GLY521, LEU384, MET388, LEU391, LEU428, PHE404, LEU387, LEU346, GLU353, LEU349 etc.

The docking scores of tamoxifen, 5-FU and VNS10 were reported to be -9.511, -5.448 and -10.001, respectively. This suggests that VNS10 has a comparable affinity for its target to the reference drug tamoxifen and 5-FU.

We have found that the both the parent compound and compound VNS10 depicted specific van der Waals (vdW) interactions with the surrounding hydrophobic and other residues LEU384, ILE424, PHE404, ARG394, MET388, MET421, THR347, LEU539. LEU391, LEU346.

The lead compound VNS10 formed π-Alkyl interactions with LEU536, ALA350, and LEU354. Triazole nucleus of lead compound VNS10 showed π-Alkyl interaction with ALA350, conventional hydrogen bonding with THR347 residue, π- σ interaction with LEU525, and π-Sulphur interaction with MET343 residue. Moreover, the napthyl ring of VNS10 showed π-anion interaction with ASP351 residue, whereas it showed π-Alkyl interaction with LEU536, LEU354 and ALA350 and π- π stacking with TRP383 residue. Terpenoid parent moiety in VNS10 undergoes alkyl interactions with LEU346, and ALA350 residues and van-der Waals

interaction with LEU384, PHE404, MET388, LEU391, LEU349, LEU387, ARG394, GLU353.

5.3.2.2 Molecular dynamic simulation studies on estrogen receptor α (ERα)

Molecular dynamic (MD) simulation study for 100 ns of protein ligand complex was performed using GROMACS 2020 in order to understand the stability and confirmational changes of complex. Based on the high docking score, the complexes of the potential ligands VNS10 with 3ERT protein, were subjected to molecular dynamic simulations. Quantitative assessments of a protein-ligand complex's stability can be derived from examining root mean square deviation (RMSD) and root mean square fluctuation (RMSF) throughout the simulation. RMSD measures the average variation in displacement of a specific group of atoms in a given frame compared to a reference frame. Dynamic studies showed that the PLA-3ERT complex remained stable during the simulation. A lower RMSD value indicates that the protein did not experience substantial conformational changes during the simulation, a conclusion further corroborated by the low RMSF values. The root mean square deviation (RMSD) value of protein rise from 0.2 to 0.45 nm for the first 20 ns and after the 20 ns it reached equilibrium and RMSD was found to be stable in the range of 0.3 -0.4 nm. Likewise, for the ligand RMSD in the Fig. 58A was observed to have jump in RMSD from 0.1 to 0.55 nm during the first ten ns later on from 10 ns onwards it seems to be stable in the range of 0.37 to 0.65 nm. Further, in order to properly estimate the dynamic behavior and the pliability of the protein during the protein ligand interaction stages of the simulation, RMSF (root mean square fluctuation) calculation was performed and illustrated in the Fig. 58B that showed the RMSF value ranges from 0.1 to 1.1 nm indicating the stability of the complex. RMSF value of ligand from the graph illustrated in Fig. 58C ranges from 0.05 to 0.25 nm suggesting the stability of the ligand in the system indicating that the compound VNS10 was actively bound with amino acid residues. Further, the average number of hydrogen bonds were calculated all around the 100 ns

simulation time with a cut-off value 0.35 and was illustrated in Fig. 58D suggesting the stability of the complex. We used the H-bond utility in GROMACS in order to calculate the average hydrogen bond distance and found an average distance 0.35 nm suggesting sufficient ligand-protein interaction. Finally, in order to determine the compactness, the radius of the gyration (rGy) for the complex was determined by utilizing the gyrate utility in GROMACS and found the value of this complex that fluctuated between 1.3-1.8 nm indicating an stable complex in Fig. 58F.

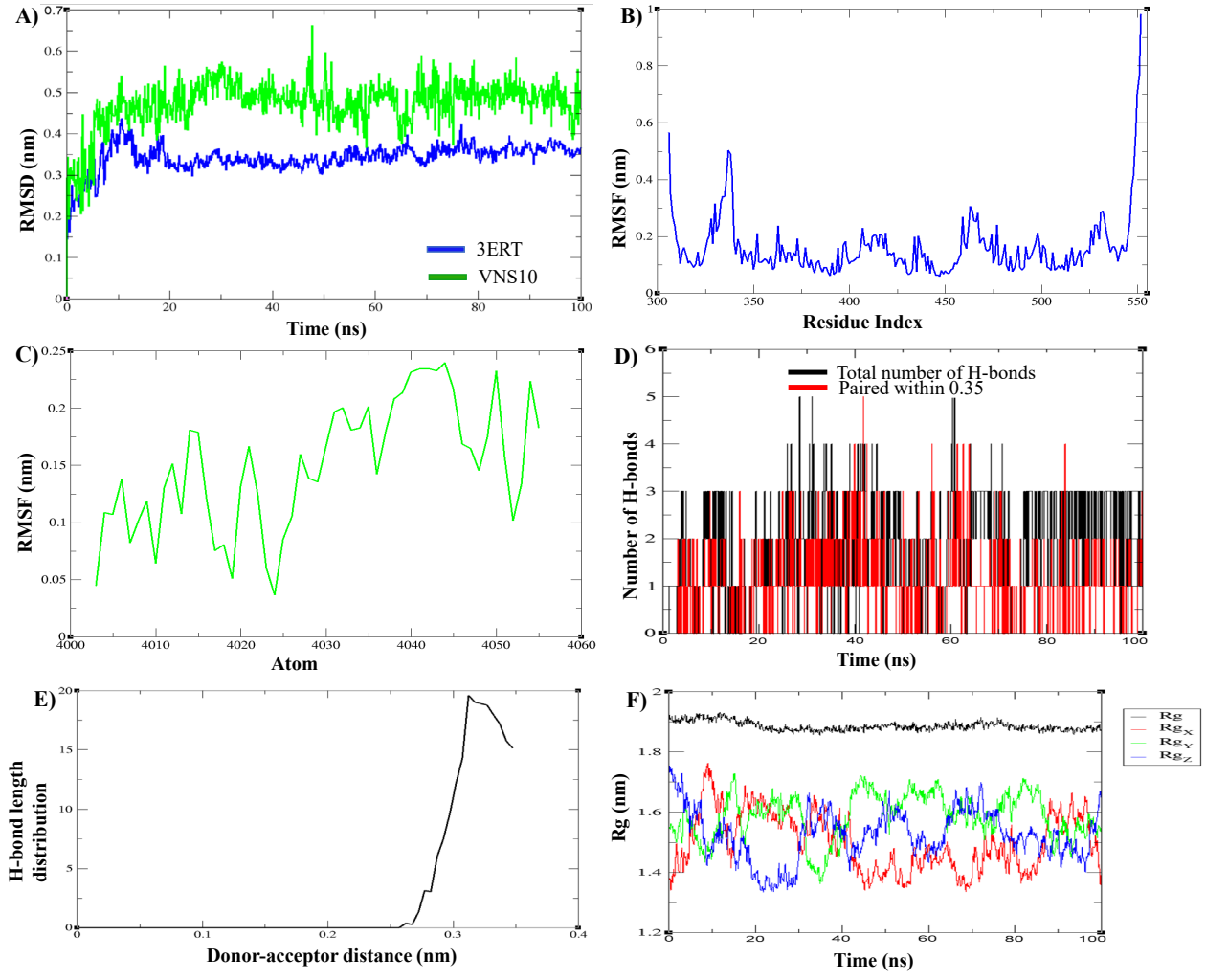

Figure 58 Molecular dynamic analysis of complex VNS10 complex, (A) depicts the protein root mean square deviation (RMSD) (left Y-axis) and ligand RMSD (right Y-axis) indicating the stability of ligand VNS10 with respect to protein ERα, (B) root mean square fluctuation (RMSF) for protein, (C) depicts the ligand VNS10 Root mean square fluctuation (RMSF) and

stability at active site, (D) depicts ligand contacts with ERα residues, and (E) showing the RMSF plot of protein ERα during simulation.

5.3.2.3 Analysis of drug-likeness, ADME, and toxicity parameters

The *in silico* ADME properties of the drugs are very important in drug discovery as the pharmacological and pharmacokinetic properties of the molecule must reach the action point in a timely manner, in sufficient concentration, and can be eliminated from the body after their action. According to Lipinski's rule of five, any molecules that follow the following parameters, i.e., hydrogen bond donors <5, hydrogen bond acceptor <10, molecular weight below 500, calculated log P < 5, can have better *in vivo* absorption.

Before evaluating the biological activity of the synthesized derivatives, *in silico* studies of synthesized compounds (VNS01-VNS23), including precursor MDL, were screened through swissADME. In addition, toxicity prediction results suggested that compounds predicted to have no toxicity in mice and rats. The cardiotoxicity (hERG) prediction indicates a low risk against the hERG channel. Most of the synthesized compounds followed the Lipinski rules and showed favorable pharmacokinetic profiles for all descriptors.

The molecular masses and calculated number of the allowed donor and acceptor hydrogen bonds of the investigated compounds with water correspond to permitted values.

The estimation of octanol-water partition coefficient (lipophilicity) studies as of Log Poctanol/water (given as consensus Log Po/w* - an average of five predictions calculated via SwissADME tool http://www.swissadme.ch/) of our compounds is in the range 2.94–3.89. The topological polar surface area (TPSA) is another important descriptor of the appropriate physicochemical space for oral bioavailability and should be in the range of 20 $Å^2$–130 $Å^2$. For the tested molecules, the values are 39.94 $Å^2$ - 85.76 $Å^2$ for all compounds. All compounds are moderately or poorly soluble in water, have high gastrointestinal absorption, and have mixed BBB permeability. There are 3 violations of lead likeness for a few compounds: the slightly

higher molecular weight MW > 350 and lipophilicity XLOGP3 > 3.5. No PAINS filter alerts were found. Synthetic accessibility was found to be high for all compounds.

5.3.3 Biological Activity

5.3.3.1 *In vitro* Antiproliferative activity

The twenty-three novel compounds (VNS01-VNS23) were assessed for their *in vitro* anticancer activity against a panel of five human cancer cell lines including, MCF-7 (Breast), MDA-MB-231 (Breast), A549 (Lungs), SiHa (Cervical), and BL60 (Melanoma) along with a normal kidney cell line (HEK-293) by employing MTT assay. Tamoxifen and 5-fluorouracil were used as positive controls. The majority of synthetic derivatives displayed better cytotoxic activity than the parent compounds on MCF7, MDA-MB-23, A549, SiHa, and BL60 cell lines.

The results indicated that all our compounds (VNS01-VNS23) exhibited strong cytotoxicity against tested five human cancer cells in micromolar concentrations. Among the tested compounds, compound VNS10 had the greatest anti-tumor activity of the tested cancer cell lines, with IC_{50} values of 2.38 ± 1.16 μM, respectively. Among synthesized derivatives, nine compounds showed anti-proliferative activities at less than 5 μM against the MCF-7 cell line. In the case of A549 and MDA-MB-231 cells, most of the compounds had less cytotoxic activities than those of 5-FU. Further, *in vitro* cytotoxicity was checked on one of the normal cell lines, HEK-293, to find the peculiarity of the compounds towards the cancer cell lines.

From the IC_{50} values, it is quite clear that almost all the active compounds exhibited less cytotoxic activity towards the normal kidney cell line (HEK-293) compared to their anticancer potential against cancer cell lines, which justifies that the triazole analogs (10 and 15) can be considered as a good lead anti-cancer agents. When compared to the cytotoxicity of the parent compound MDL (IC_{50} 35.2 ± 2.50 μM), this indicates that triazolyl MDL derivatives prepared from MDL could make better ligands with improved cytotoxicity against cancer cell lines.

5.3.3.2 Acridine orange/ethidium bromide staining

The acridine orange/ethidium bromide (AO/EB) staining procedure was followed to differentiate live, apoptotic, and necrotic cells. To further understand whether the inhibition is through apoptosis or through non-specific necrosis, the morphological abnormalities were studied by acridine orange/ethidium bromide staining (AO/EB) induced by most active compounds VNS10 and VNS15 against MCF-7 cells in a concentration-dependent manner. Acridine orange stains the nuclei green, permeating through the cell membrane, whereas ethidium bromide is taken up only when the membrane permeability is compromised, staining the nuclei red. The cells treated with the compounds VNS10 and VNS15 and untreated MCF-7 cells were stained with acridine orange and ethidium bromide and were analyzed under a fluorescent microscope. As demonstrated, both compounds VNS10 and VNS15 significantly induced apoptosis after 48 h co-treatment with tested compounds at the indicated concentrations compared with the untreated control group.

The nuclei of untreated cells appeared like intact, normal structures, while signs of apoptosis-like condensed chromatin and destructive fragmentation of nuclei were observed in the cells treated with compounds VNS10 and VNS15, which have shown significant nuclear changes at concentrations 1.5, 3, and 6 μM which were absent in untreated cells.

5.3.3.3 Intracellular ROS production assay

The ROS level was determined qualitatively by using a cell-permeant probe 2,7-dichlorodihydrofluorescin diacetate (H2DCFDA). Increased levels of intracellular reactive oxygen species (ROS) are a prime indication of apoptosis in cancer cells and, eventually, cell death. To examine increased levels of ROS, we investigated the effect of the compounds on intracellular ROS generation through fluorescent dye, 2'-7'-dichlorodihydro-flurescien diacetate (DCFH-DA) in MCF7 cells.

DCFH-DA is a non-fluorescent cell-permeable dye which, upon oxidation by intracellular esterases in the cytosol, converts to nondiffusible green fluorescent DCF. The results from the quantitative analysis revealed that the compounds VNS10 and 15 induced elevations of ROS levels compared to control at a concentration of 1.5, 3, and 6 μM.

The amount of ROS was increased after the treatment with compounds VNS10 and VNS15 at the mentioned concentrations. Observation through a fluorescence microscope is a qualitative means of ROS generation in MCF-7 breast cancer cells where a sharp increase in fluorescence intensity was observed. This study indicated that compounds VNS10 and VNS15 triggered ROS generation in MCF-7 cells, which is a key feature of apoptosis.

5.3.3.4 AnnexinV-Alexa Fluor/Propidium iodide staining assay

In order to determine the cell death, annexin V-Alexa Fluor and propidium iodide staining were performed by using the Annexin V-Alexa Fluor apoptosis detection kit according to the manufacturer's protocol (Sigma Aldrich). The AnnexinV- Alexa Fluor /Propidium Iodide staining was performed in MCF7 cells to quantify the percentage of apoptotic cells through a flow cytometer. This assay facilitates the detection of live cells (Q1-LL; AV-/PI-), early apoptotic cells (Q2-LR; AV+/PI-), late apoptotic cells (Q3-UR; AV+/PI+)) and necrotic cells (Q4-UL; AV-/PI+).

As found, in line with their anti-proliferative activity, the tested compounds were effective in triggering apoptosis in MCF-7 cells, and the proportion of early and late apoptotic cells was also quantified accordingly. The results have manifested that in the cells when treated with compound VNS10, the percentage of early and late apoptotic cells increased from 10.27% (control) to 27.42%, 61.22%, and 81.28%. Hence, the results have stipulated that the compound VNS10 induced apoptosis in the dose-dependent manner.

5.3.3.5 Cell cycle analysis

The great potential of compound VNS10 in inducing apoptosis in MCF-7 cells motivated us to investigate the change of cell cycle distribution induced by compound VNS10. After 24 h co-incubation with the tested compounds, the cells were collected and analyzed via flow cytometry.

Flow cytometric analysis was done to determine the percentage of the cell population in different cell cycle phases. Many of the cytotoxic compounds show cell inhibitory activity by halting the cellular progression by arresting the cell cycle at a specific check point that has been an ideal option for developing potential chemotherapeutic agents. In order to elucidate the role of the compound VNS10 on the progression of the cell cycle, cell cycle analysis through flow cytometry was performed. From the cell cycle analysis results, we could find that the compound VNS10 has shown a slight increase in the G2/M phase population of cells treated at 1.5 μM and 3 μM concentrations compared with the control. The results showed that the percentage of MCF-7 cells in the G2/M phase from 7.38% in control increased to 11.08% and 26.26% at 1.5 μM and 3 μM concentrations, respectively. Hence, the compound VNS10 exerted its cell inhibition by arresting the cell cycle at the G2/M phase, and compound VNS10 induced apoptosis, gradually preventing cell proliferation. In sum, all these results indicated that compound VNS10 induced a concentration-dependent G2/M stage arrest of MCF-7 cells. Taken together, these findings suggest that the tested compound induced cell apoptosis by arresting the cell cycle.

5.4 Conclusion

The preparation of natural product derivatives and their biological screening are important aspects of synthetic and medicinal chemistry that may lead to the discovery of new therapeutic agents. Because of its unique biochemical properties, MDL deserves further investigation in the field of oncology. Click chemistry is the most fascinating and effective approach for the

generation of drug candidates. Several research groups used click chemistry as a synthetic tool for the generation of valuable scaffolds to achieve new biological knowledge.

The chemistry which involves copper(I)-catalyzed 1,2,3-triazole formation from azides in the terminal acetylenes is a powerful tool for the generation of privileged medicinal scaffolds, due to its high degree of dependability, complete specificity, and the biocompatibility of the reactants. The synthetic route that we follow to construct the new derivatives i.e. 1,2,3-triazole analogues of MDL (VNS01 to VNS23) is exhibiting in (Scheme 1).

The desired 1,2,3-triazole hybrids (VNS01-VNS23) were achieved by a three-step protocol with propargylation followed by Huisgen's 1,3-dipolar cycloaddition reaction without isolation of potentially unstable organic azide. Initially, compound 1(MDL) was treated with propargyl bromide in presence of sodium hydride in dry THF under inert environment to afford the intermediate 2 in very good yield (93%). Parallelly, in step 2 substituted aromatic azides were prepared by according to the literature procedures using aromatic boronic acids and anilines. In step 3, intermediate 2 was treated with substituted azides in presence of sodium ascorbate and $CuSO_4.5H_2O$ in H_2O-t-BuOH solution (1:1, v/v) to afford 1,4-substituted 1,2,3-triazoles (1-23) in good to very good yields (60-92%). All the synthesized compounds were purified by column chromatography and thoroughly characterized by their spectral analysis (IR, ^1H & ^{13}C NMR and HRMS).

The ^1H NMR of final compound 3-25 showed a singlet in the range δ 7.89-8.31 ppm assigned to proton of 1,2,3-triazole ring and absence of acetylenic proton in IR spectrum indicating the acetylenic proton is converted into 1,2,3-triazolic proton, O-CH_2 singlet in the range δ 5.19-5.43 ppm; aromatic protons in the range δ 6.40-8.50 ppm and methyl protons in the range δ 1.24-2.49 ppm. The confirmatory evidence of the 1,2,3-triazole ring was also obtained from the ^{13}C NMR, which displayed a signal in the range δ 125-148 ppm.

Further, preliminary drug likeness properties of the newly synthesized molecules were determined by *in silico* SwissADME online property calculation software and the data obtained were presented. For most compounds, the parameters like hydrogen bond acceptor, hydrogen bond donor, rotatable bonds (n-rotb) were in the range of Lipinski's rule of 5.

The structure of compound VNS08 was unambiguously confirmed and studied in detail by X-ray diffraction analysis. The single-crystal X-ray diffraction study of compound VNS08 confirmed the assigned structure of the product. Compound crystallizes in the monoclinic space group. All the structures were finally confirmed from ESI HRMS displaying desired molecular ion peak. Apoptosis is a form of cell death which involves the activation of different caspases and other signalling molecules for the programmed death of the cell. We performed apoptosis assay to examine the effect of VNS10 on apoptosis. Upon treatment with VNS10, morphological changes like nuclear cleavage, membrane blebbing, chromatin condensation and cell shrinkage were distinct under microscope showing hallmarks of apoptosis. Interestingly, we observed a sufficient number of cells undergoing apoptosis even at much lower concentration of VNS10 in comparison to positive control Tamoxifen. Further, detailed *in vivo* pharmacological investigations can be carried out for the lead compound VNS10 to develop it as effective anti-cancer agent.